1970

Process system safety limits of the MITR-II.

Luxford, Bruce

Massachusetts Institute of Technology

PROCESS SYSTEM SAFETY LIMITS OF THE MITR-II

Bruce Luxford

PROCESS SYSTEM SAFETY LIMITS OF THE MITR-II

by

BRUCE LUXFORD

Lieutenant, U.S. Navy

B.S., University of Illinois

(1964)

Submitted in Partial Fulfillment

of the Requirements for

the Degrees of

NAVAL ENGINEER

and

MASTER OF SCIENCE

(Nuclear Engineering)

at the

Massachusetts Institute of Technology

June, 1970

PROCESS SYSTEM SAFETY LIMITS OF THE MITR-II

by

BRUCE LUXFORD

Submitted to the Department of Naval Architecture and Marine Engineering on June 4, 1970, in partial fulfillment of the requirement for the degree of Naval Engineer and to the Department of Nuclear Engineering on June 4, 1970, in partial fulfillment of the requirement for the degree of Master of Science.

ABSTRACT

The process system operating limits of the MIT Reactor redesign (MITR-II) are based on measurable parameters, i.e., primary coolant flow rate, bulk outlet temperature, and reactor power. The limits are conservatively established to maintain the fuel plate clad surface temperature at the hot spot below 250°F. Operation of the reactor within these limits is intended to preclude any possibility of boiling in the core. The nuclear properties of the reactor are examined first to determine the power production within the reactor and within a single fuel element.

Emphasis of this study focuses on the hottest element and, further, the hottest fuel plate. Attention is given to the effects of control rod height on the relative variations in the radial and axial neutron flux and power density distributions. The coefficient of convective heat transfer at the fuel plate surface is evaluated. Engineering hot channel factors are also included in the calculations to account for departures from nominal design resulting from fuel element manufacturing tolerances and uncertainties in power, flow, and heat transfer measurements. Consideration is also given to the flow rate of the secondary H_2O coolant from the cooling towers necessary to remove the reactor heat load.

Under the most adverse operating conditions, limits of 1800 GPM minimum primary coolant rate, 155°F maximum bulk outlet temperature, and 6 megawatts maximum reactor power are established. These are the limits such that the reactor could be safely operated with these parameters simultaneously approaching their limits and still fulfill the criterion that no boiling occur in the core.

Thesis Supervisor: David D. Lanning
Title: Professor of Nuclear Engineering

Thesis Supervisor: James W. Gosnell
Title: Assistant Professor of Nuclear Engineering

ACKNOWLEDGEMENTS

Thanks are due to Professor D.D. Lanning and Professor J.W. Gosnell for their guidance and constructive comments on all phases of this study, and to Mr. E.J. Barnett for helpful discussions.

The author was fortunate to have capable assistance during the various parts of this work. It is therefore with pleasure that the author acknowledge the contributions of Messrs. Andrews K. Addae and Paulo M. Furtado.

The author is indebted to Mrs. Jean Fairneny and Miss Rita Falco for a neat preparation of the manuscript and figures.

TABLE OF CONTENTS

TABLE OF CONTENTS

(Continued)

LIST OF FIGURES

LIST OF TABLES

Chapter 1

INTRODUCTION

Since its completion in the Spring of 1958, the MIT Reactor has served as a vital educational and research facility for the Massachusetts Institute of Technology and the scientific community. Based on technical obsolescence, however, it was predicted that the reactor life would be approximately ten years. Consequently, a redesign group was formed to consider renovation of the reactor to make it more technically competitive with newer reactors which have been designed and built since the MIT Reactor. The general methods and procedures for carrying out such a renovation were inherent in the original reactor design and have been active for approximately two years to permit the introduction of a new type of core unique to this reactor, designed to increase the available neutron fluxes in the experimental facilities by a factor of somewhere between three and five.

The redesign section of the reactor is almost entirely confined to the upper plug section and the core tank section of the original design. In the redesign, as shown in Figure 1.1, the core is light water cooled and moderated, and the moderator for the reflector is heavy water as was the case in the original reactor. The hexagon shaped core (see Figure 2.1) is contained in a cylindrical aluminum tank with the annular space between the hexagon and the cylindrical tank

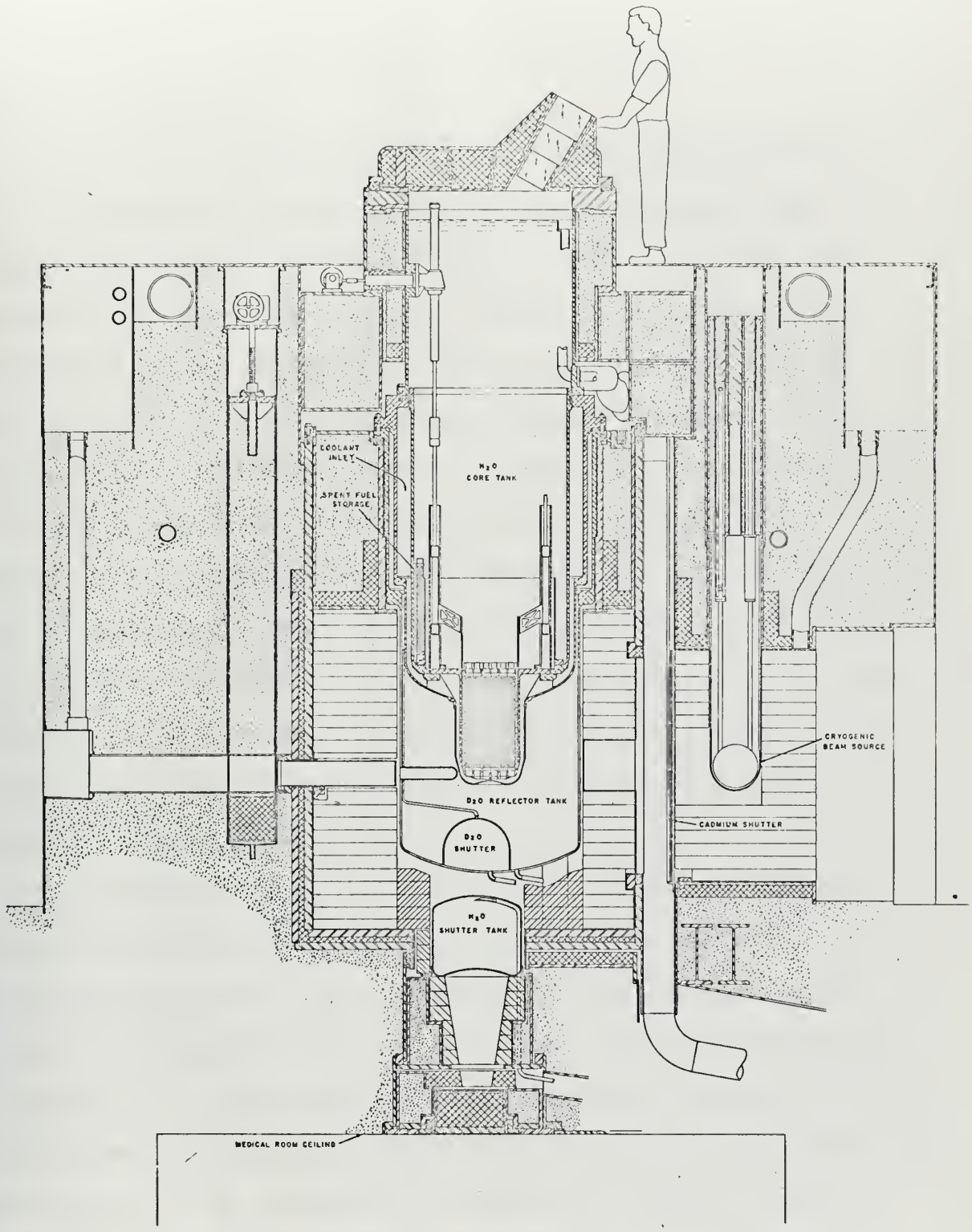

VERTICAL SECTION THROUGH MITR-II

FIGURE 1.1

used for the light water entrance channels. Six flat plate control rods are located around the core between the fuel and the D_2O reflector.

One of the primary purposes for redesigning the MITR was to accommodate a compact core configuration in order to obtain large thermal neutron fluxes in the beam tube near the bottom of the reactor core. Almost by definition, the achievement of a high thermal flux in the reflector at the beam tube will be accompanied by a sharply increasing flux gradient near the bottom of fuel plates. The lower portion of the fuel plates will consequently have a high power density. It, therefore, becomes imperative that the power density in the core does not exceed such limits as to cause boiling within the core. Hence, the objective of this study: determine, on the basis of experiments and theoretical calculations, the process system operating limits of the MIT Reactor redesign (MITR-II).

The redesign basis for the MITR-II evolved around the thermal hydraulic characteristics of the fuel element from the requirements that the installed primary coolant pumps and heat exchangers are to be used, and that the reactor is to operate at a power level of five megawatts without boiling in the core. To allow for some latitude for the operation of the reactor, it is necessary to establish limits on the measurable reactor operating parameters, i.e., minimum

coolant flow rate, maximum bulk outlet temperature, and maximum reactor power. The process system safety limits define these parameters such that the reactor can safely operate with these parameters simultaneously approaching their limits and insure that no boiling of any type will occur within the core.

Chapter 2

DESCRIPTION OF THE MIT REACTOR

2.1 General

The MITR-II is a light water cooled and heavy water reflected reactor for research and educational purposes at the Massachusetts Institute of Technology. The reactor will be operated at power levels up to five megawatts, although the nuclear and structural design anticipates that higher power levels are possible.

2.2 Core

The reactor core is a hexagon, 13.3 inches across the flat as shown in Figure 2.1. It consists of three concentric hexagonal rings of fuel with 15 elements in the outer hexagon, 9 elements in the next hexagon, and 3 elements in the center. Each of the 27 tightly packed elements consists of 15 fuel plates held by aluminum side plates in a rhombic shape as shown in Figure 2.2. The core height is approximately 29 inches.

The inner hexagon ring containing 3 elements is surrounded by a fixed, hexagon shaped, aluminum clad cadmium shim located at the inner edge of the hexagonal rib. This thin plate absorber will be placed into a hexagonal shelf extending down from the top of the core 14 inches.

The outer two hexagon rings containing 24 elements is divided into three identical regions. Each region is

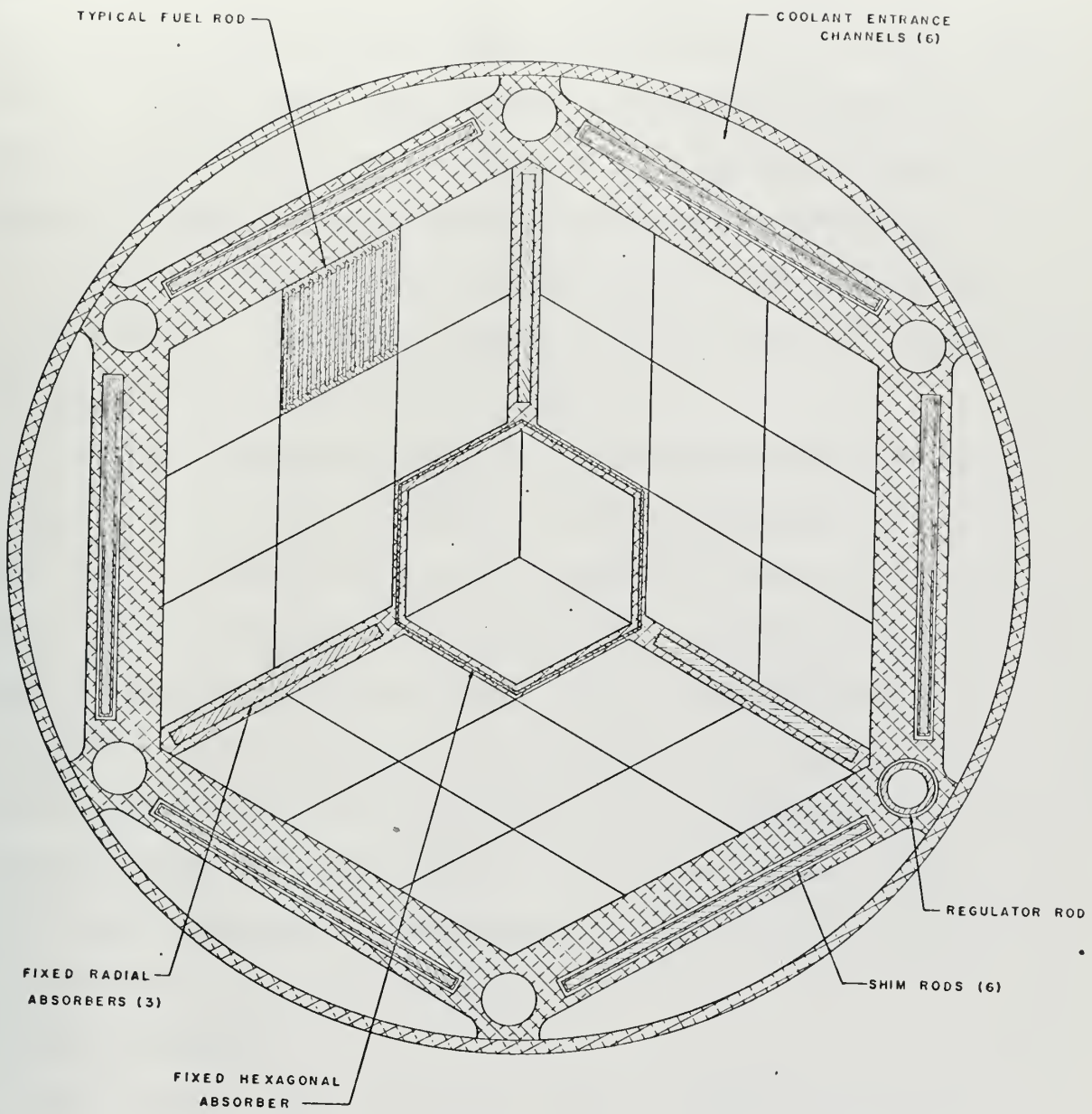

HORIZONTAL SECTION THROUGH MITR-II CORE

FIGURE 2.1

flanked by aluminum clad cadmium absorber plates located in slots in the radial ribs of the core support structure. These plates, also, extend down from the top of the core 14 inches. At the outer edge of each region are located two movable shim blades, for a total of six blades, in slots around the edge of the hexagonal core support structure.

A regulating rod is located in one of the small holes at the corner of the core support structure and is located generally toward the thermal column side.

The core hexagonal support structure is connected to an upper tank 4 feet in diameter and approximately 7 feet high, and is mounted on its own flange and bolted to an extension near the neck of the core tank. It serves as the support for the core itself and for the essential part of the control rod mechanisms. In addition, the support is the alignment plate for the control blade mechanisms and all key components of these systems are bolted to work through this single structure. The weight of this unit is carried by the upper tank.

2.3 Fuel Elements

The MITR-II fuel elements, shown in Figure 2.2, are specially designed and fabricated for the high flux, dense geometry core. As indicated in the drawing, the element is rhombic in shape with a total width along the side of the

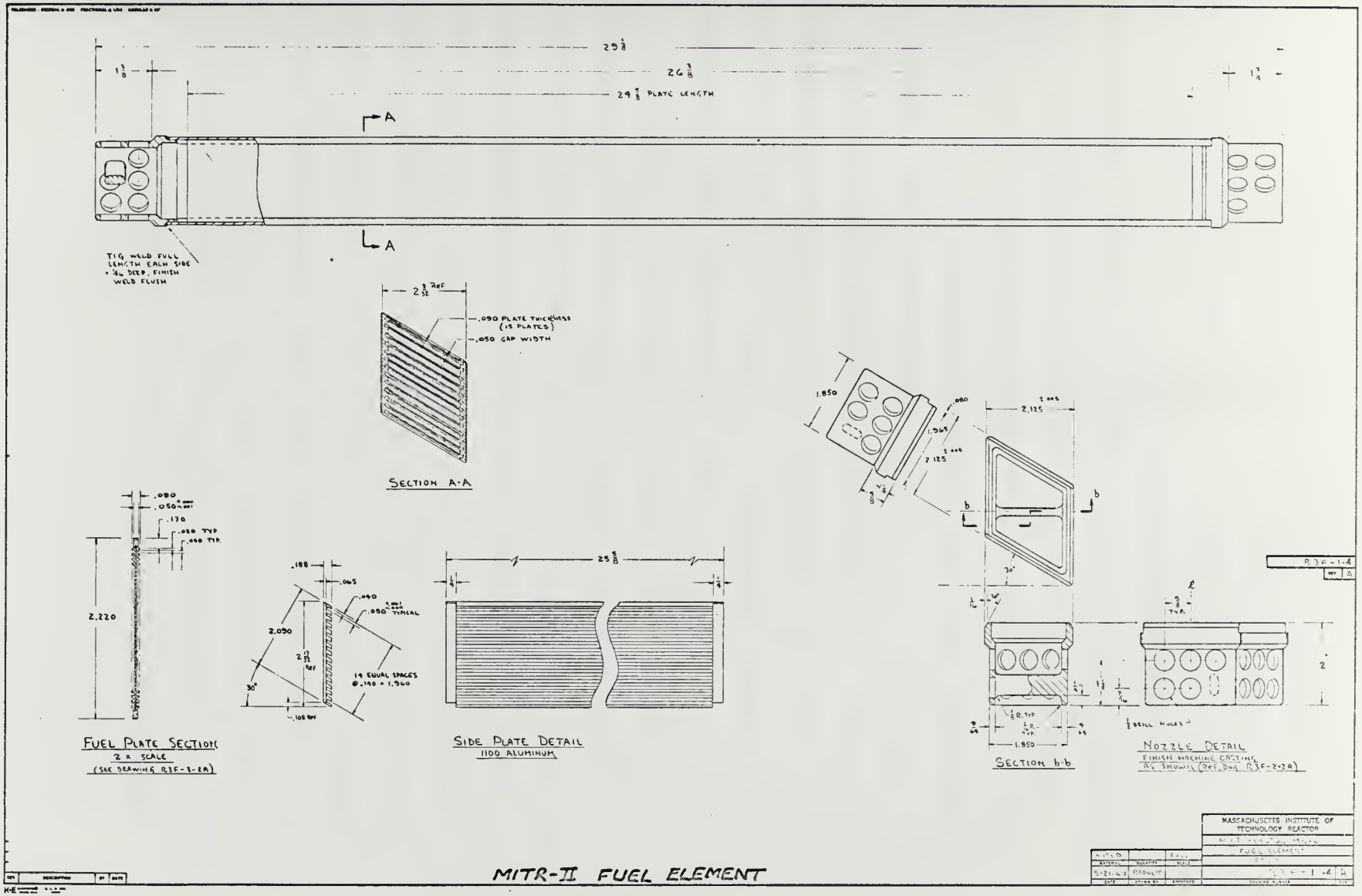

MITR-II FUEL ELEMENT

FIGURE 2.2

flat of 2-1/2 inches. The overall length including the end nozzles is 29-1/2 inches. The fuel element consists of 15 straight fuel plates assembled between two grooved side plates which are 0.188 inch thick and 2.500 inches wide. The fuel bearing plates are 0.090 inch thick with longitudinally milled coolant fins on both sides so as to produce a 20 mil land, 20 mil groove and 20 mils in depth. The overall dimensions of the fuel-bearing plates are 2.220 inches wide, 24.625 inches long, and they are spaced 0.140 inch apart to form 16 cooling water passages 0.050 inch wide. The spacing is maintained by grooves in the side plates and the end nozzles which are designed to provide structural rigidity for the element. Each element has an end nozzle at either end and is completely reversible, allowing it to fit into the lower matrix and to mate with the upper hold-down grid.

The fuel element contains 240 $\pm$ 4.8 grams of U-235. In any individual plate, the amount of U-235 does not exceed 16 $\pm$ 0.48 grams. Each plate contains a core of approximately 93% enriched uranium alloyed with pure aluminum. This core is 23-1/4 $\pm$ 3/16 inches long, 1-3/4 $\pm$ 1/16 inches wide, and 0.020 inch thick and is clad on all surfaces with 6061 aluminum alloy. The minimum thickness on the face plate is 0.015 $\pm$ 0.001 inch with a permissible scratch depth of 0.003 inch. The minimum amount of aluminum cladding the nearest

edge of the core alloy and the edge of the fuel plate is 0.204 inch.

2.4 Control Rods

The MITR-II contains six shim safety blades, a single fine regulating rod, 3 fixed flat neutron absorbers located in the radial ribs of the core support structure, and a hexagonal shaped fixed shim located at the inner edge of the hexagonal rib surrounding the three inner fuel elements, all shown in Figure 2.1. The purpose of these various absorbers is to maximize the flux and power densities in the lower half of the core and to give ease to nuclear control. The shim blades are arranged symmetrically with respect to the core, while the regulating rod is located in one of the small circular holes at the corner of the hexagonal core structure.

Each shim blade consists of a rectangular plate of 40 mil cadmium clad with 6061 aluminum for a total thickness of 1/4 inch, and is attached to an arm. This arm, in turn, is attached to a weighted member of low hydraulic cross section which operates in a guide tube bolted to the inner core structure plate. The blades are raised through a magnetic coupling by motors situated just below the top deck plate. Loss of magnet current causes the heavy member and the attached control element to drop. As the control blade moves downward into its flat slot, water in slot exits through holes at the corners of the water release from the

bottom of the guide tube for the carrier rod.

Preliminary calculations indicate that the total reactivity worth of the movable neutron absorbers is approximately:

Shim blades: 14.5 β (See Appendix A)

Regulating rod: Less than 1.0 β

The maximum possible variable excess reactivity for five megawatt operation will be limited such that the reactor can always be kept in a shutdown condition with only four of the six shim blades inserted.

The fixed absorbers extend down from the top of the core about 14 inches. Each absorber is cadmium sheathed with aluminum, and each is held down completely by the upper core hold-down grid. The primary purpose of these fixed absorbers is to insure that the reactor can go critical and can operate at the desired power level and flux distribution.

2.5 Primary Coolant System

The H_2O primary system, as shown in Figure 2.3, is used as a coolant and moderator in the MITR-II. The system consists of a single loop which contains two parallel pumps, two parallel heat exchangers and associated valves, piping, and instrumentation. The pumps and heat exchangers may be operated singly, in parallel, or cross connected. The main suction and discharge lines to the

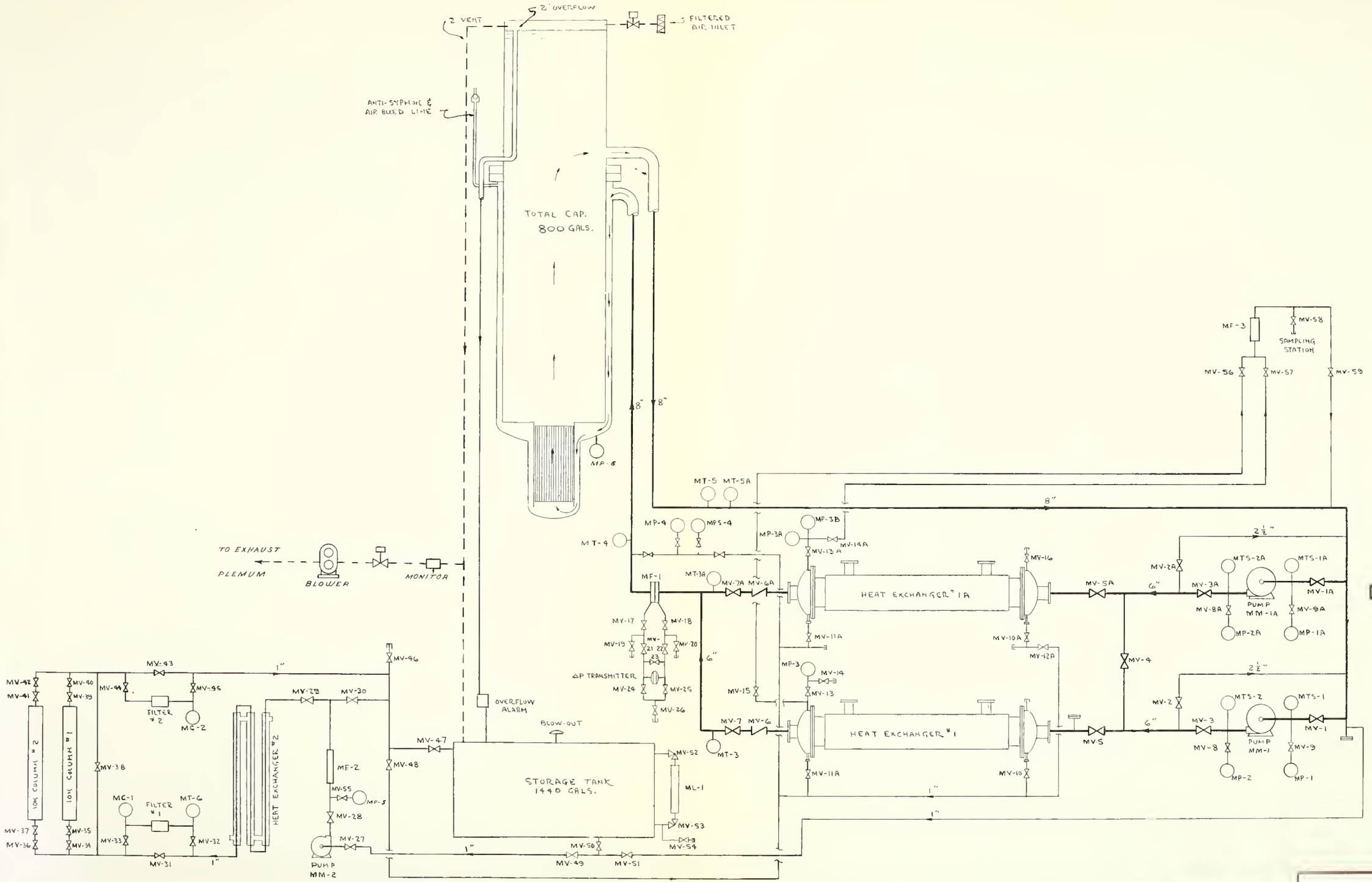

FIGURE 2.3
PRIMARY FLOW SYSTEM

reactor tanks each use an 8 inch pipe so only two pipe runs and two tank penetrations are needed.

Starting at the pumps, light water is pumped through single stage, horizontally mounted, stainless steel centrifugal pumps rated at 1200 GPM at a head of 80 feet and is powered by a 40 HP motor. Normal discharge pressure is 55 psi. The discharge from the pumps goes to the tube side of the main heat exchangers. The heat exchangers are composed of 885 tubes of 3/8 inch O.D. and is of the single pass type. The tubes are 18 BWG thick and are constructed of stainless steel. They are mounted on a 1/2 inch square pitch and are 14 feet, 2 inches long. The outside area of the tubes is approximately 1230 square feet. The shell is 18 inches in diameter and incorporates 9 baffles. It is designed for a free flow area of 67 square inches. The pressure at the outlet of the tube side of the heat exchangers is 43 psi, and each heat exchanger has a nominal capacity of 3×10^6 BTU/hr.

The 6 inch lines leaving the heat exchangers join into a single 8 inch line, containing a flow nozzle and, down stream near the inlet plenum, an anti-syphon valve that prevents emptying of the core tank in case of rupture to the main inlet line. The pressure at the inlet plenum is 23 psi. The inlet plenum is designed to give a fan shaped plume

entering the annular space between the core tank and the core support shroud tank. The flow then moves downward to the core tank and is then directed up through the core and into the shroud tank toward the outlet plenum where it is drawn through the outlet line to the suction side of the main coolant pumps. The pressure drop across the core is approximately 8 psi at the flow rate of 80.9 GPM per element (2200 GPM, total). The pump suction pressure is 8 psi.

2.6 D_2O Reflector

The moderator for the reflector is heavy water as was the case in the original MIT Reactor. The D_2O is contained in a 4 ft. diameter tank, which also contains re-entrant thimbles for the horizontal beam ports. A single large pipe from the heavy water tank permits rapid dumping of the heavy water reflector, providing a secondary safety feature for shutdown. Flow of D_2O into the reflector tank is provided by means of the large pipe which contains the dump valve provision. The exit pipe and the external system, which will include a pump and small heat exchanger, will be of relatively small size as it is anticipated that not more than 250 kilowatts will be deposited (generated) in the D_2O reflector.

2.7 Secondary Coolant System

The secondary H_2O coolant system is designed to remove the heat load from the reactor core and reflector primary

coolant as well as the heat load from the shield and experimental primary coolant. The system contains the pumps, piping and valves, heat exchangers, cooling towers and all instrumentation necessary to insure safe operation under all anticipated conditions. Operation at power levels greater than 2 megawatts require that two secondary H_2O pumps and heat exchangers be run in parallel.

Cool secondary H_2O is taken from the basin of the two cooling towers through a common 10 inch pipe penetrating the containment shell into the equipment room where the flow again separates to the two pumps. These pumps discharge to the shell side of the two main heat exchangers as well as to the D_2O reflector heat exchanger, the shield coolant heat exchanger, and the experimental coolant heat exchanger. The exit flow from all the heat exchangers combines in a single 10 inch pipe which leads out of the containment shell and then separates into the return lines for each of the two cooling towers.

The cooling tower is provided with a bypass valve so that the amount of water fed to the spray top of the cooling towers for evaporation is continuously variable from zero to full flow. Varying the amount of water being bypassed from the top to the basin controls the equilibrium temperature of the entire system during different seasons of the year.

2.8 Reflector Coolant System

The reflector coolant system is designed to remove the heat deposited in the heavy (D_2O) water reflector and to maintain a high purity of heavy water. The system consists of a water pump, heat exchanger, piping and valves, and associated instrumentation for operation. Suction is taken directly from the reflector tank, and then pumped through the D_2O reflector heat exchanger where heat is transferred to the secondary H_2O coolant. The heat exchanger discharge is through an 8 inch dump line above the dump valve and up through the dump line to the reflector tank.

The heavy water cleanup loop is designed to insure a constant heavy water reflector level during normal operation and to maintain the heavy water inventory at a high purity. The heavy water is kept pure by using two filters and a mixed bed ion exchanger with associated piping, pump, valves, heat exchanger and associated instrumentation.

2.9 Shield Coolant System

The shield coolant system removes heat deposited in the lead thermal shield which surrounds the graphite reflector and thermal column. For cooling purposes, the thermal shield is divided into four separate regions, each with two sets of stainless steel coils embedded within. Only one coil in each region is used for heat removal, the second coil acting as a spare.

The system uses demineralized water supplied by an integral distilled water storage tank. The heat exchanger, which transfers heat to the secondary H_2O coolant system, is of a double pass type with 438 U-shaped tubes with a total length of 3 ft., 1/4 inch I.D. and 24 gage thick. A centrifugal pump is used for circulation and an ion column is used to maintain a high purity of distilled coolant water.

The above paragraphs outline the properties of those sections of the MITR-II with which this paper is primarily concerned.

Chapter 3

POWER PRODUCTION DISTRIBUTION

Introduction

The objective of the work described in this section was to determine the power production distribution within the core as a whole and within a single fuel element. The general method followed was to investigate the neutron flux distribution and the power production by using available mathematical models and computer programs. The calculations described in this section are based upon the power density distributions determined by A.K. Addae (1) using the EXTERMINATOR-2 (2) computer code.

This analysis procedure first homogenizes the core into a two-dimensional, cylindrical array and determines the properties at the various points within the reactor array. Three neutron energy groups and the homogenized properties were used in the EXTERMINATOR-2 code to determine the relative variations in neutron fluxes and power density distributions from which the location of the hottest element is found and the relative magnitude of its heat generation established.

In this section the methods are described for shifting from the homogeneous model to the heterogeneous reality, the value of the heat flux distribution among the plates of the element is then established for a total reactor power of six

megawatts, and the hottest fuel plate is found and its power distribution calculated.

3.1 Homogenized Core Properties

Homogenization of the reactor is accomplished, assuming a cylindrical geometry, by dividing the reactor into 1944 regions. The regions are formed by dividing the axial height into 54 rows and the radial distance into 36 concentric annular rings; the divisions in either the axial or radial directions are not necessarily equal. The core itself takes up 25 rows and 9 annular rings, the remainder of the regions accounting for the reflector, shield, and structural members (e.g., the reflector tank).

A partial listing of the input data necessary for the EXTERMINATOR-2 is given below:

Number of groups

Microscopic cross sections

Radial and axial mesh spacing for each region

Nuclide concentration

Region composition

From the input, the macroscopic cross sections, diffusion coefficients, and scattering matrix is computed for each group and composition. The number of reactions, e.g., absorptions, productions, fissions, and scatters, is also given for each group and composition.

The calculation of reactor power must begin with an analysis of the energy released in the fission of U-235. The total energy released in the fission of U-235 may be expressed as

$$E = 193.8 + E_c \text{ (Mev)} .$$

The value of 193.8 Mev/fission is obtained from the generally accepted distribution of fission energy of U-235 (3); see Table 3.1. E_c is the energy released per fission resulting from neutrons being captured in the materials of the reactor.

Table 3.1

DISTRIBUTION OF FISSION ENERGY: U-235

Source	Mev/Fission
Kinetic energy of fission fragments	168.0
Kinetic energy of fission product decay β's	7.0
Kinetic energy of fast (fission neutrons)	5.0
Prompt gamma rays	7.8*
Fission product decay gammas	6.0**
Total	193.8

*6.48 - 1 Mev photons, 1.17 - 3 Mev photons, 0.14 - 5 Mev photons, and 0.01 - 7 Mev photons (4)

**6 - 1 Mev photons (5)

There is also approximately 11 Mev of neutrino energy per fission which accompanies the β decay, but this energy is not recoverable by the reactor.

The value of E_c depends upon the amount of type of materials in the reactor. The EXTERMINATOR-2 output includes the macroscopic cross sections from which we can determine the energy released (per fission) per neutron captured by considering the following:

$$\left.\frac{\text{Energy}}{\text{Fission}}\right|_{\text{nuclide}} = \frac{\text{Energy}}{\text{Capture}} \times \frac{\Sigma_{\text{capture}}(\text{nuclide})}{\Sigma_{\text{absorption}}(\text{composition})} \times \frac{\text{No. of absorptions in composition}}{\text{total number of fissions}}$$

Table 3.2 lists the capture gamma energies of the various MITR-II materials. The capture cross section of D_2O is quite low and has been neglected in these calculations. The Q-value for the $B^{10}(n,\alpha)Li^7$ reaction is 2.792 Mev (6); the ratio of absorptions in the boral to the total number of fissions is 0.1014, yielding 0.283 Mev/fission from the (n,α) reaction.

Table 3.3 lists the energy per fission released for each material in the reactor. The total energy released per fission is equal to

$$E = 193.8 + 12.78 = 206.58 \text{ Mev/fission.}$$

3.2 Radial and Axial Flux Variations

Figures 3.1 and 3.2 show the thermal flux distributions for shim blade heights (from bottom of core) of 11.70 inches

Table 3.2

CAPTURE GAMMA ENERGIES OF MITR-II MATERIALS

Material	Photon Energy	Energy/Capture	Total Energy/Capture
Al (7)	1 Mev	3.252 Mev	
	3	2.323	
	5	1.834	
	7	2.095	9.054 Mev
U-235 (8)	1	0.8	
	3	6.0	6.8
H_2O (9)	2	2.22	2.22
Cd (10)	1	3.761	
	3	3.801	
	5	1.263	
	7	0.212	9.043
Graphite (11)	5	4.95	4.95
Boral (12)	1	0.48	0.48*

*Does not include the $B^{10}(n,\alpha)Li^7$ reaction.

Table 3.3

CALCULATED ENERGY RELEASED PER FISSION

FOR EACH NEUTRON CAPTURED

Material	Mev/Fission	
U	4.75	(capture gamma only)
Al	3.98	
Boral	0.33	(includes both (n,α) and (n,γ) energies)
Graphite	0.20	
Cd	2.87	
H_2O	0.65	
Total	12.78	

and 6.70 inches respectively for the reactor operating at six megawatts. It is important to note that as the control rods are lowered, higher fission densities occur in the lower, active portion of the core.

A considerable portion of the fission neutrons leak from the core into the heavy water reflector where they are slowed down resulting in the thermal neutron flux being a maximum in the reflector near the core edge. The power-distribution, therefore, peaks at the edge of the core.

A basic formula for power in a homogenized core is

$$P = K \int_{vol} \Sigma_f \phi dV$$

where

$$K = 3.3095 \times 10^{-17} \frac{\text{Mw-sec}}{\text{fission}} .$$

This constant was computed by using a fission yield of 206.58 Mev which includes 12.5 Mev/fission of capture gammas as calculated in the previous section. The macroscopic cross section, Σ_f, is known to be zero everywhere except in the fuel regions. The integral may therefore be approximated by a summation over the individual fuel regions.

$$P = K \sum_{i=1}^{n} \left(\sum_{j=3}^{3} \Sigma_{f_{ij}} \bar{\phi}_{ij} \right) V_i .$$

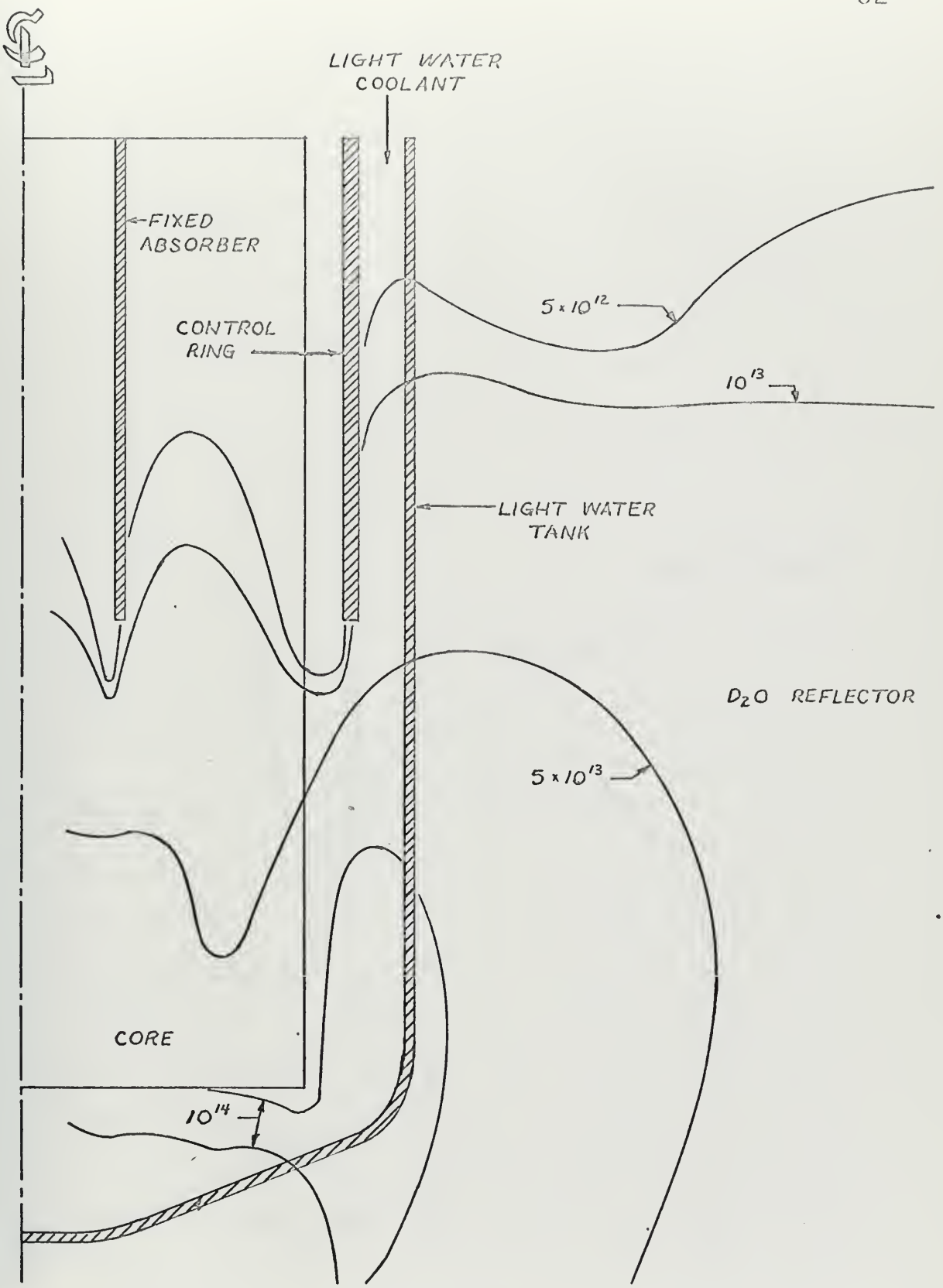

Figure 3.1 THERMAL NEUTRON FLUX (N/CM^2-SEC)
SHIM BLADE HEIGHT: 11.70 IN.

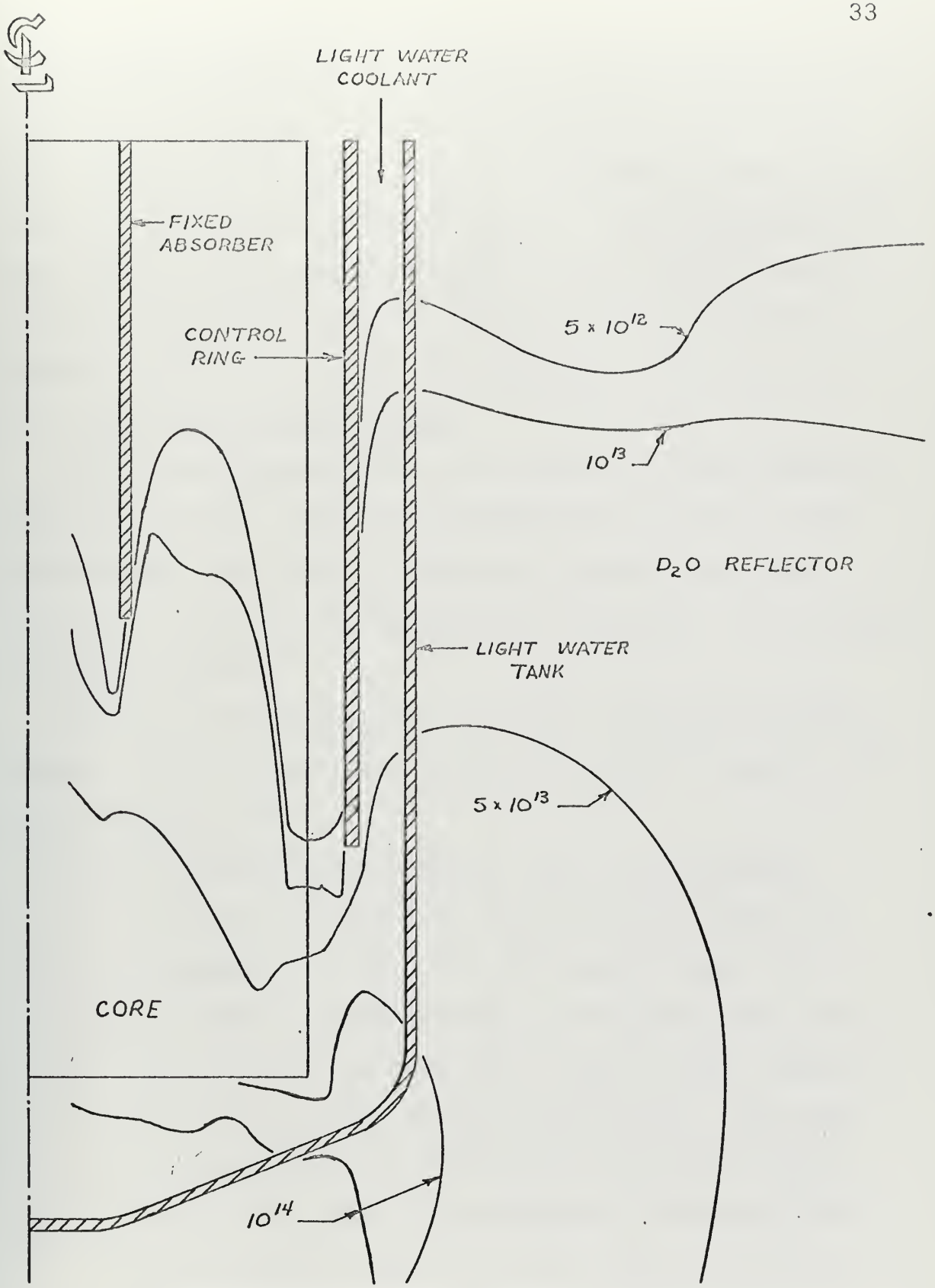

Figure 3.2 THERMAL NEUTRON FLUX (N/CM^2-SEC)
SHIM BLADE HEIGHT: 6.70 IN.

In this expression Σ_f is defined for the volume of the fuel region. $\bar{\bar{\phi}}_{ij}$ is the volume averaged flux in the i^{th} fuel region and j^{th} energy group. As a volume average, $\bar{\bar{\phi}}_{ij}$ contains both radial and axial factors. The EXTERMINATOR-2 code computes the integrated power in each annular region, making it unnecessary at this time to calculate the flux factors.

3.3 Power Produced Per Element

The average power in the fuel region is known from the homogeneous model. From the EXTERMINATOR-2 output of integrated power, the transition must now be made from the homogeneous model to the heterogeneous reality. The procedure is outlined below:

The heat flux normal to the finned clad in the heterogeneous core at a specified axial mesh point is computed in the following manner:

1) The EXTERMINATOR-2 output gives the integrated heat flux parallel to the vertical (z) axis of homogenized core. The differential heat flux is found by subtracting the integrated heat flux at one vertical mesh point from the heat flux at the next highest adjacent mesh point. The average power density, PAV, generated between adjacent mesh points is calculated by dividing the differential heat flux by the vertical distance between adjacent mesh points.

2) The power density generated in the fuel meat, PDM, is calculated by multiplying the average power density, PAV, by the ratio of total horizontal cross-sectional area of a unit homogenized element to total horizontal cross-sectional area of fuel in a heterogeneous element, i.e.,

$$\text{PDM} = \text{PAV} \times \frac{\text{horizontal cross-sectional area of homogenized element}}{\text{horizontal cross-sectional area of fuel in a heterogeneous element}} .$$

3) The heat flux normal to (one side of) the finned clad is then

$$Q/A = 0.5 \times \text{normalization factor} \times \text{PDM} \times \text{thickness of fuel meat (20 mils)}$$

where the normalization factor includes factors for the fraction of energy (per fission) deposited in the core, 95% (see Section 4.3), and converts BTU/sec cm^2 to BTU/hr ft^2. The factor 0.5 accounts for one-half of the generated power leaving one face of the fuel plate normal to the finned clad.

4) The value of the heat flux, Q/A, is plotted against the axial distance along the fuel plate, and is then numerically integrated to find the total power produced within the fuel element and the

average heat flux, q''_{AVG}, for each plate in the element.

Following the procedure outlined above on the EXTERMINATOR-2 output of integrated power, it is observed that the three central elements produce the most power per element within the core. With the reactor at six megawatts of power and the assumption that 95% of the power is deposited in the core (including the gamma heating in the moderator and fuel elements), each central element produces 230.54 kilowatts of power. (Derivation of the fission energy distribution is given in Chapter 4).

3.4 Power Produced in the Hottest Fuel Plate

In addition to the method described above (i.e., numerical integration of Q/A over the axial distance), the average power generated in each fuel plate can be calculated by dividing the power produced in each element by 15, the number of plates per element. In order to compute the power produced in the hottest fuel plate, both the axial and radial power peaking factors must be computed.

The local axial power peaking factors are found by dividing the local heat flux at equally spaced mesh points by the average heat flux, q''_{AVG}. Table 3.4 lists the maximum axial power factors, F_a; the magnitude of $(F_a)_{max}$ is large because the power in the upper portion of the core is negligible in comparison with the power in the lower, more active

part of the core, and the calculation of the average power includes the power in the upper portion.

The radial peaking factors are calculated using the EXTERMINATOR-2 output and preliminary studies made by A.K. Addae (13) using the PDQ-7 (14) computer code. (The PDQ-7 code is used to compute the radial neutron flux variation in a hexagonal geometry.) Since the PDQ-7 hexagonal geometry solution is only a two-dimensional result, typical of the EXTERMINATOR-2 run with the shim blades 11.70 inches from core bottom, the radial peaking factors for varying rod heights were calculated from the PDQ-7 result by proportioning the result with the various EXTERMINATOR-2 results, i.e.,

$$F_r(i^{th} \text{ case}) = F_r(\text{base case from PDQ-7}) \times \frac{F_r(i^{th} \text{ case from EXTERMINATOR-2})}{F_r(\text{base case from EXTERMINATOR-2})}$$

where: base case implies shim blade height of 11.7 inches from core bottom.

Table 3.4

SUMMARY OF RADIAL AND AXIAL POWER FACTORS

Shim Blade Height (in. from bottom)	EXTERMINATOR-2 F_a	EXTERMINATOR-2 F_r	PDQ-7 F_r
11.70	3.242	1.111	1.167
9.28	3.399	1.194	-
6.70	3.531	1.296	-

Applying the radial factor obtained from the PDQ-7 program to the fuel in the hottest element, it is assumed that the hottest fuel plate produces

$$1.167\ (15.37) = 17.94\ \text{KW} \quad .$$

Since all of the calculations are aimed at removing the heat from the hottest plate and limiting its temperature, the sources of uncertainties must also be considered. These uncertainties will be discussed in more detail in Chapter 4.

Chapter 4

PRIMARY COOLANT FLOW

Introduction

All parameters from the core configuration through the reactor temperatures to the primary coolant flow rate are completely interdependent. The power production in the hottest plate, derived as shown in Chapter 3, is used in this chapter to calculate the limitations on the fuel plate and bulk coolant temperatures. Once reasonable ranges of values of these parameters are established, limits on the minimum coolant flow, maximum bulk outlet temperature, and maximum reactor power are calculated such that the reactor can be operated with these parameters simultaneously approaching their limits and no boiling occurs.

4.1 Determination of the Convective Heat Transfer Coefficient

Experimental work by Spurgeon (15) enabled Furtado (16) to derive the heat transfer coefficient in the manner described below for longitudinally finned fuel plates. The experimental program to measure the heat transfer coefficient consisted of a test section designed to support a 0.090" x 2.5" x 25.5" rectangular coolant channel which was electrically heated by two 12 volt, 1500 ampere generators connected in series. Cooling water was pumped through the channel at rates varying from 1.5 to 5.0 GPM. The analysis

of the longitudinal fin data by Furtado differed from that reported by Spurgeon, numerical solution of the heat conduction equation was made (including the electrical heating of the fins), giving the temperature distribution on the test section. The heat conduction equation in finite difference form is equivalent to a system of linear equations; this system was solved by the Gauss-Jordan reduction method (computer program). Furtado's boundary conditions were:

1) back plate adiabatic
2) heat transfer coefficient arbitrarily selected
3) coolant bulk temperature equal to zero.

A correlation was developed among the temperature drop across the test section ΔT, the heat transfer coefficient h and the amount of heat, Q, conducted through the test section. The final form of Furtado's expression is:

$$\Delta T = \frac{Q}{A_p}\left[\frac{1}{\eta h} + \frac{t_{eff}}{K}\right] \qquad (4.1)$$

where ΔT = difference between the average temperature of the back plate and coolant temperature, ^{o}F

Q = power generated on the test section, BTU/hr

A_p = back plate surface area, ft^2

h = convective heat transfer coefficient, $BTU/hr^{o}F\ ft^2$

t_{eff} = thickness of equivalent flat plate test section, ft

K = thermal conductivity of test section material, $BTU/hr^{o}F\ ft$

η = fin effectiveness defined as the effective area of the finned plate surface divided by the area of the back plate surface.

Furtado's conclusion is that the convective heat transfer coefficient for longitudinally finned test sections is conservatively fit by using the Colburn correlation:

$$Nu = 0.023\ Re^{0.8} Pr^{0.3} \qquad (4.2)$$

where $Nu = hD_e/K$

$Re = \rho v D_e/\mu$

$Pr = \mu C_p/K$

(v = coolant velocity, ρ = density, μ = viscosity)

and D_e is the equivalent flow diameter taken as $(4A/P)$ where A is the flow area and P is the channel perimeter. The design of the longitudinally finned fuel element can be established on the basis of the calculated fin effectiveness and the standard heat transfer correlations.

4.2 Core Temperature Limitations

The principal factor affecting the allowable temperatures at various points in the core is the requirement that the melting point of the fuel plates not be approached under any conceivable circumstances. To provide as large a safety margin as possible, all specifications have been written so that no boiling of any type is allowed to occur.

In effect, this means that no nucleate boiling is allowed at the surface of the fuel plates. The wall temperature at the hottest spot of the hottest plate of the central element must therefore be limited.

The hot spot on the fuel plate is close to the radial centerline of the core. The value of $(T_{wall})_{max}$ allowable is first approximated as the onset of incipient boiling at the static pressure at the fuel bottom. The coolant head is 135 inches when the level is at the reactor scram point of four inches below the normal overflow level. At this pressure, the saturation temperature is 226.8°F under no-flow conditions and is higher when the primary coolant is flowing.

Based upon a semi-theoretical approach, Bergles and Rohsenow obtained a correlation (17) for predicting incipient boiling that is dependent only on pressure and wall temperature. For water over a pressure range from 15 to 2000 psia, the heat flux at incipient boiling is given by:

$$q''_{IB} = 15.6\ P^{1.156}(T_{WIB} - T_{SAT})^{2.30/P^{0.0234}} \qquad (4.3)$$

where: q''_{IB} = incipient boiling heat flux, BTU/hr ft^2,

P = pressure, psia,

T_{WIB} = local wall temperature at incipient boiling, °F,

T_{SAT} = fluid saturation temperature, °F.

When the absolute pressure is taken to be 14.7 + 4.87 (135 in. of water) = 19.57 psia, Eq. (4.3) becomes:

$$T_{WIB} = 226.8 + \left(\frac{q''_{IB}}{485.6}\right)^{0.466} \qquad (4.4)$$

It will be seen in Section 4.4 that the hottest peak plate temperature occurs at the coolant channel inlet (fuel bottom). This position is taken as the core hot spot and the operating limits are established on the basis that the plate surface temperature in this position, $(T_{wall})_{max}$, does not reach the boiling temperature, T_{WIB}.

4.3 Reactor Heat Load

In this section, the amount of energy produced and absorbed in the various regions of the reactor is reviewed in order to determine the total amount of reactor heat produced per fission in the core and the fraction of this heat that is removed by the primary coolant.

As pointed out in Section 3.1, the heat generated in a nuclear reactor is directly or indirectly derived from the energy released in nuclear fissions. Of the energy released, the following assumptions are made:

1) The kinetic energy of the fission fragments and fission product decay β's is absorbed in the fuel elements.

2) The energy released in the capture of a neutron in the boral shield is absorbed in the shield.

3) Approximately 75 percent of the gamma and fast neutron energy absorbed in the D_2O reflector is removed by the D_2O circulating system.

4) The capture gamma energy produced in the graphite reflector is absorbed in the graphite reflector and the shield.

The gamma spectrum from fission may be calculated from the data listed in Tables 3.1 and 3.3; Table 4.1 summarizes the gamma energy distribution and its source.

The fraction of gamma radiation escaping from the core was calculated by assuming a homogenized, self-absorbing spherical source. Price, Horton, and Spinney (18) states that the fraction (probability) of gamma radiation escaping an absorbing sphere of radius R is given by:

$$\text{Fraction (probability) of escaping} = f(\mu,R) = \left.\frac{\text{Attenuated gamma current}}{\text{Unattenuated gamma current}}\right|_{\text{at R}},$$

where: μ is the effective linear absorption coefficient,

$$\text{Non-absorbing current} = \frac{SR}{3},$$

$$\text{Absorbing current} = \frac{S}{4\mu}\left[1 - \frac{1}{2\mu^2R^2} + e^{-2\mu R}\left(\frac{1}{\mu R} + \frac{1}{2\mu^2R^2}\right)\right];$$

Table 4.1

CALCULATED GAMMA ENERGY DISTRIBUTION PER FISSION

Photon Energy	Source	Mev/Fission	Total
	Al	1.36	
	U-235 (n,γ)	0.56	
1	Boral	0.05*	15.59
	Cd	1.19	
	Fission product decay γ's	6.00	
	Prompt gammas	6.48	
	Al	0.97	
	U-235	4.19	
3	H_2O	0.65	8.19
	Cd	1.21	
	Prompt gammas	1.17	
	Al	0.77	
5	C	0.20*	
	Cd	0.40	1.31
	Prompt gammas	0.14	
	Al	0.88	
7	Cd	0.07	0.96
	Prompt gammas	0.01	
		Total	26.05

*not included in total

hence,

$$f(\mu,R) = \frac{3}{4\mu R}\left[1 - \frac{1}{2\mu^2R^2} + e^{-2\mu R}\left(\frac{1}{\mu R} + \frac{1}{2\mu^2R^2}\right)\right] . \quad (4.5)$$

In order to calculate the effective linear absorption coefficient for the core, the volume fractions of the constituents is used, as shown in Eq. (4.6):

$$\mu = \mu_{Al}V_{Al} + \mu_u V_u + \mu_{H_2O}V_{H_2O} + \mu_{Cd}V_{Cd} , \quad (4.6)$$

where: μ_i = linear absorption coefficient of material i,

V_{Al} = volume fraction of aluminum = 0.437662,

V_U = volume fraction of uranium = 0.034506,

V_{H_2O} = volume fraction of water = 0.510805, and

V_{Cd} = volume fraction of cadmium = 0.017027;

(note that μ_i is dependent upon the gamma energy).

The total core volume was taken to be 9551.067 cubic inches (for a core height of 30.25 inches and diameter of 19 inches), yielding a spherical radius of 33.43 cm. Table 4.2 summarizes the gamma radiation escaping from the core.

For comparison, a homogenized cylindrical, self-absorbing source was assumed, and the fraction escaping calculated. The difference between the spherical and cylindrical assumptions was less than 4 percent.

The fuel elements and moderator absorb the gamma energy that does not escape from the core. The division of this energy was established by considering the ratio of the absorption coefficients and volume fraction of the materials within the core. The H_2O will absorb $(\mu_{H_2O} V_{H_2O}/\mu) \times 100$ percent of the gamma energy, and is summarized in Table 4.2.

Table 4.2

SUMMARY OF GAMMA ABSORPTION

Photon Energy (Mev)	Fuel Elements (Mev/fission)	Moderator (Mev/fission)	Reflectors and Shield (Mev/fission)
1	6.30	1.50	10.21
3	3.18	0.80	1.89
5	0.66	0.13	0.37
7	0.47	0.08	0.26
Total	10.81	2.51	12.73*

*does not include capture gammas in graphite or boral

To compute the fraction and location of energy deposited by the fast (fission) neutrons, the fast neutron (Group 1) macroscopic removal cross-section and flux output from the EXTERMINATOR-2 data was used. The total number of removals from the high energy neutron group to a lower energy group is found by summing the product of the flux, (macroscopic) removal cross section, and volume over each composition of the core, i.e.,

Total number of removals from Group 1

$$= \sum_{\text{composition } i} (\Sigma_{r1} \phi_1 V_i)$$

The fraction of fast neutrons slowed down in the moderator, reflector and shield is the ratio of the removals in the respective composition to the total number of removals. The energy deposited by the fast neutrons is then just the product of the total kinetic energy of the fast (fission) neutrons and the fraction of removals in each composition. Table 4.3 lists the summary of fast neutron energy deposition.

Table 4.3

FAST (FISSION) NEUTRON ENERGY DEPOSITION

Location	Fraction of removals	Kinetic energy (per fission) of fast neutrons removed (Mev)
Core (Moderator)	0.9117	4.56
Reflector	0.0874	0.44
Shield	0.0009	Negligible
Total	1.0000	5.00 Mev/ fission

Table 4.4 is a summary of the above data, the distribution of fission energy. Assuming that approximately 25% of the energy deposited in the reflector and shield is conducted into the core tank, then the heat load on the primary coolant is

Table 4.4

DISTRIBUTION OF ENERGY RELEASED IN

THE REACTOR PER FISSION

Location and Source	Mev/fission	Percentage
Fuel elements		
K.E. of fission fragments	168.00	
K.E. of β particles	7.00	89.95%
Gamma energy	10.81	
Moderator		
K.E. of fast neutrons	4.56	3.42%
Gamma energy	2.51	
Reflectors and Shield		
K.E. of fast neutrons	0.44	
Gamma energy	12.98	6.63%
$B^{10}(n,\alpha)Li^{7}$ reaction	0.28	
Total	206.58	100%

approximately 95 percent of the reactor power, If, instead, a fraction of the energy deposited in the core is conducted to the reflector and shield, then the figure of 95% is reduced accordingly. The figure of 95% will be used, however, as a conservative basis in determining the operational limits of the reactor.

4.4 Hot Spot Calculations

For a conservative design, engineering hot channel factors have been established to account for small dimensional deviations from the nominal design of the reactor fuel elements resulting from manufacturing tolerances, for departures from ideal flow conditions, and for uncertainties in power, flow and heat transfer measurements. The uncertainties are elaborated below.

The factor F_H is defined as the ratio of the maximum channel mixing-cup enthalpy rise to the enthalpy rise in a channel of nominal dimensions and flow rate located in a region of average volumetric heat generation. The enthalpy rise rather than the temperature rise is used for simplicity and generality, since it avoids the problems of varying specific heat.

The factor F_θ is defined as the ratio of maximum film temperature difference to the average film temperature difference calculated for a core composed entirely of

nominal channels. F_θ is used for the determination of maximum surface heat flux in the reactor core to the average surface heat flux computer for a core composed of all nominal channels.

4.4.1 Power Density Variation

The estimated uncertainty in the power distribution is ± 10%. The enthalpy and heat flux terms are increased by 1.10 to account for the uncertainty.

4.4.2 Reactor Power Measurement

It is estimated the reactor power calibration will be accurate to within 5%. The enthalpy and heat flux terms are increased by 1.05.

4.4.3 Channel Dimensional Tolerances

The hot spot temperature rise due to the channel dimensional tolerance will occur in a channel of minimum thickness where the local plate thickness is a maximum. Ignoring the entrance and exit effects and considering only the friction within the channel, the hot channel factors are calculated as follows:

Enthalpy term, F_H, is increased by $\left(\frac{d_{nom}}{d_{min}}\right)^{5/3}$,

Film temperature difference term, F_θ, is increased by

$$\left(\frac{d_{max}}{d_{min}}\right)\left(\frac{d_{nom}}{d_{min}}\right)^{1/3},$$

where: d = channel thickness,

nom = nominal value = 0.090 in.,

min = minimum value = 0.0855 in., and

max = maximum value = 0.0945 in.

The values of F_θ and F_H are given in Table 4.5.

4.4.4 Plenum Chamber Flow

The particular geometry of the reactor inlet plenum and the entrance regions to the individual coolant channels gives rise to a small inequality in the flow distribution among the channels. An experimental mockup was made for a single fuel element to determine the flow inequality, and the increases in the enthalpy and film temperature difference factors are 1.08 and 1.06 respectively.

4.4.5 Fuel Plate Eccentricity

If the fuel meat is separated from the coolant by a cladding material, variations in the thickness of the cladding around the perimeter of the heat transfer surface of the fuel plate due to manufacturing tolerances will cause variations in the heat flux distribution at the heat transfer surface compared to the symmetrical case. The factor which accounts for this deviation is called the eccentricity factor.

The hot spot eccentricity factor for the fuel plate is calculated by computing the ratio of the heat flux from the thin clad side of a plate with the maximum allowable eccentricity

to the heat flux from a nominal plate. By simple application of the heat conduction equation under the conservative assumption of equal bulk coolant temperatures on both sides of the plate, the result is

$$F_H = 1 + \frac{\bar{a}_{max} - a_{nom}}{\frac{K_c}{K_M} b + a_{nom} + \frac{K_c}{h}} = 1.001 ,$$

and

$$F_\theta = F_Q = 1 + \frac{a_{max} - a_{nom}}{\frac{K_c}{K_M} b + a_{nom} + \frac{K_c}{h}} = 1.003 ,$$

where: K_c = thermal conductivity of clad,

K_M = thermal conductivity of meat,

h = convective heat transfer coefficient,

b = fuel plate meat half-thickness,

a_{nom} = nominal fuel clad thickness in the core,

a_{max} = maximum fuel clad thickness in the core,

$\bar{a}_{max}$ = maximum average fuel clad thickness in any one channel

4.4.6 Fuel Core Alloy Variation

The total fuel content of each loaded fuel plate is 16.0 ± 0.48 gm U-235. The allowable variation then is approximately 2.6% for the length of the plate and 5% for the thickness of the plates. The enthalpy term is accordingly increased by 1.026, and the film temperature difference and heat flux factors increased by 1.05 to account for variations

in the total energy generation in a fuel plate due to U-235 loading.

4.4.7 Fuel Element Tolerances

The precision of the velocity distribution measurements was 4%. Since the velocity is proportional to the square root of the measured quantity (velocity head) the uncertainty in velocity is 2%. The film temperature difference and heat flux factors are increased by 1.02.

4.4.8 Heat Transfer Coefficient Deviation

In the determination of the convective heat transfer coefficient (Section 4.1), Furtado recommends the use of the Colburn correlation with a maximum negative deviation of 20%. The deviation results in increasing the film temperature difference factor term by 1.20.

Table 4.5 summarizes the hot channel factors discussed above. The product relation between the individual and total hot channel factors is used because it must be assumed for safety that the worst manufacturing tolerances all occur at the point of maximum neutron flux.

4.5 Operational Limitations

In Chapter 3, the power produced in the hottest fuel plate and the variation in heat flux and the radial and axial power peaking factors were established for a total reactor power of 6 megawatts. In the preceeding section, the hot channel factors were calculated. In order to

Table 4.5

SUMMARY OF HOT CHANNEL FACTORS

Enthalpy factors	
Plenum chamber flow	1.08
Channel tolerances	1.089
Reactor power measurement uncertainty	1.05
Power density measurement uncertainty	1.10
Fuel density tolerances	1.026
Eccentricity	1.001
Total, F_H	1.395
Film temperature difference factors	
Plenum chamber flow	1.06
Channel tolerances	1.124
Fuel element tolerances	1.02
Fuel density tolerances	1.05
Eccentricity	1.003
Heat transfer coefficient deviation	1.20
Total, F_θ	1.536
Heat flux factors	
Fuel element tolerances	1.02
Fuel density tolerances	1.05
Eccentricity	1.003
Reactor power measurement uncertainty	1.05
Power density measurement uncertainty	1.10
Total, F_Q	1.241

establish the maximum allowable reactor power, consistent with the maximum allowable clad surface temperature, the hot channel factors were incorporated to determine their effect in the parameters involved.

The MACABRE (19) computer code was used to perform the parametric study to determine the effects in the heat flux, clad temperature, and local (channel) bulk coolant temperature adjacent to the hottest plate due to variations in the average heat flux, radial and axial power factors, coolant flow rate, and the hot channel factors. When the hot channel factors were introduced into this study, the following changes were made to the MACABRE input:

$$(q''_{AVG})_{\text{hot channel}} = F_Q \times (q''_{AVG})_{\text{nominal}}$$

$$(h)_{\text{hot channel}} = (h)_{\text{nominal}}/F_\theta$$

$$(W)_{\text{hot channel}} = (W)_{\text{nominal}}/F_H$$

where:

$(q''_{AVG})_{\text{nominal}}$ = average heat flux through the hottest fuel plate, BTU/hr ft^2

h = convective heat transfer coefficient, BTU/hr ^oF ft^2

W = flow rate through the channels adjacent to hottest fuel plate, GPM.

The average heat flux through the hottest fuel plate is calculated by dividing the power produced in the hottest plate (17.94 Kw) by the effective area of the finned plate surface (both sides). To decide what values of the total primary coolant flow rate and inlet temperature should be used for the MACABRE input, the limiting flow rate of 1800 GPM for the operating MIT Reactor and an inlet temperature of 116°F were used as a foundation.

Figures 4.1 and 4.2 are plots of the MACABRE output. Figure 4.1 shows the variation of heat flux with axial position along the hottest fuel plate for a total flow rate of 1800 GPM and a total reactor power of 6 megawatts. Curves 1 and 2, Figure 4.1 include hot channel factors whereas Curves 3 and 4 do not include hot channel factors. Curves 1 and 3 and 2 and 4 are for shim blade heights (from bottom) of 6.70 and 11.70 inches respectively. As can be seen, the uncertainties (hot channel factors) increase the maximum heat flux by approximately 24 percent in each case; this corresponds to the value of F_Q (1.241).

Figure 4.2 shows the variation of the clad surface temperature (T_{wall}) and local (channel) bulk coolant temperature with axial position along the hottest fuel plate for a reactor power of 6 megawatts, primary coolant flow rate of 1800 GPM, an inlet temperature of 116°F and hot

Figure 4.1

AXIAL HEAT FLUX DISTRIBUTION
ALONG HOTTEST FUEL PLATE
(Reactor Power: 6 Mw + Primary Coolant Flow Rate: 1800 GPM)

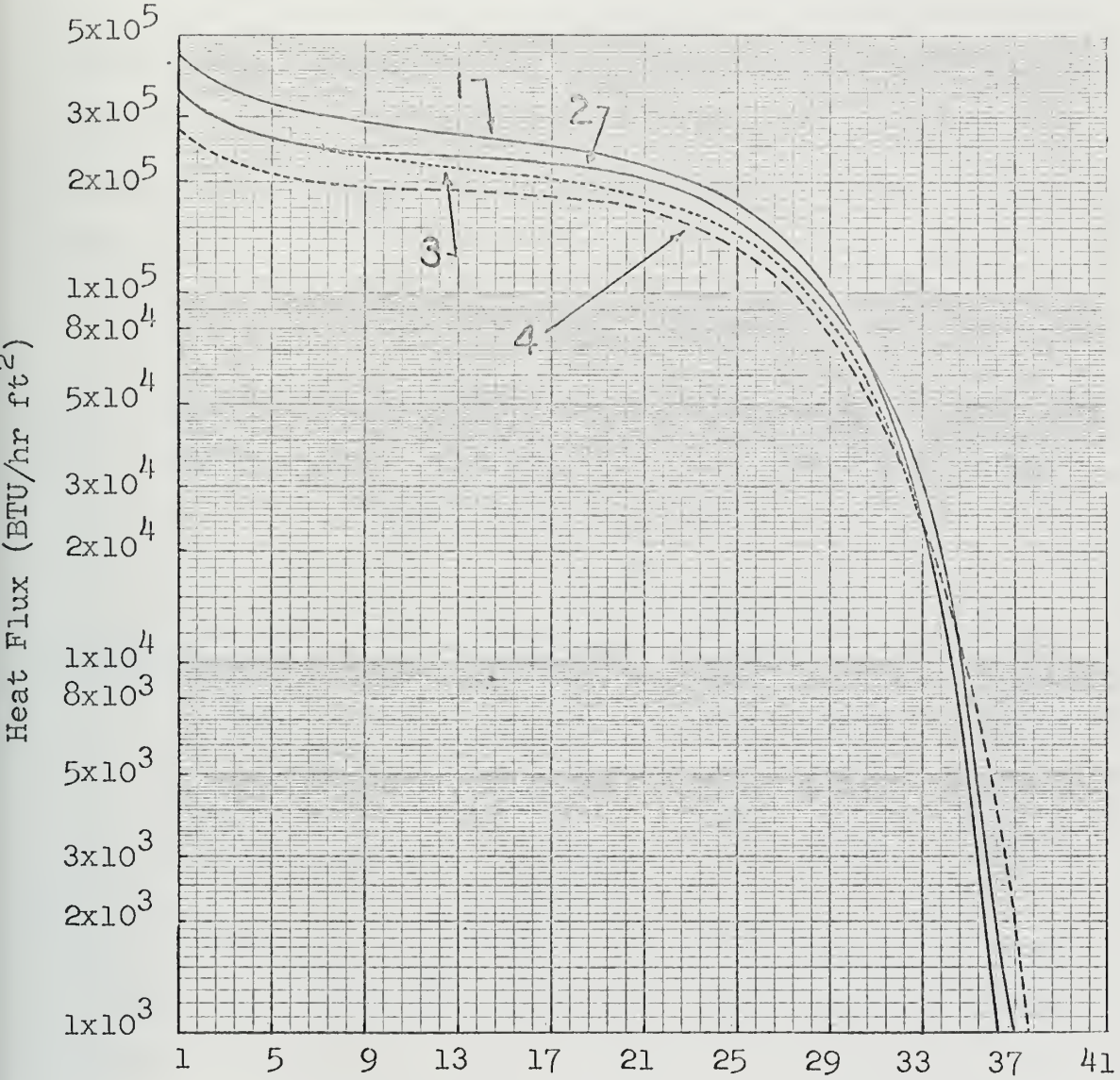

DISTANCE FROM BOTTOM OF FUEL (INCREMENTS)
(1 INCREMENT = 0.03192 FT)

	Hot Channel Factors	Shim Blade Height (In)
Curve 1	Yes	6.70
Curve 2	Yes	11.70
Curve 3	No	6.70
Curve 4	No	11.70

channel factors included. Curves 1, 2, and 3 are for rod heights of 6.70, 9.28, and 11.70 inches respectively. One might first suspect that incipient boiling occurs for the cases when the rod heights are 6.70 and 9.28 inches since the maximum wall temperature exceeds the fluid saturation temperature. Using Eq. 4.4 and the values of $(Q/A)_{max,hot\ channel}$ from Figure 4.1, the wall temperature at which incipient boiling occurs, T_{WIB}, is calculated and the results listed in Table 4.6.

Table 4.6

SUMMARY OF MAXIMUM CLAD WALL TEMPERATURES, MAXIMUM HEAT FLUXES, AND INCIPIENT BOILING TEMPERATURES FOR VARIOUS ROD HEIGHTS*

Rod height (inches from bottom)	$(T_{wall})_{max}$ ^{o}F	$(Q/A)_{max}$ (BTU/hr ft^2)	T_{WIB} (^{o}F)
6.70	241.3	4.37×10^5	250.6
9.28	227.4	3.89×10^5	249.3
11.70	214.3	3.42×10^5	248.0

*Reactor power of 6 megawatts, primary coolant flow rate of 1800 GPM, inlet temperature of 116°F, and hot channel factors included.

From Table 4.6 it is seen that the maximum wall temperature is always less than the incipient boiling temperature. To determine the maximum allowable inlet temperature such

Figure 4.2

AXIAL VARIATION OF CLAD SURFACE AND
LOCAL (CHANNEL) BULK COOLANT TEMPERATURES
ALONG HOTTEST FUEL PLATE

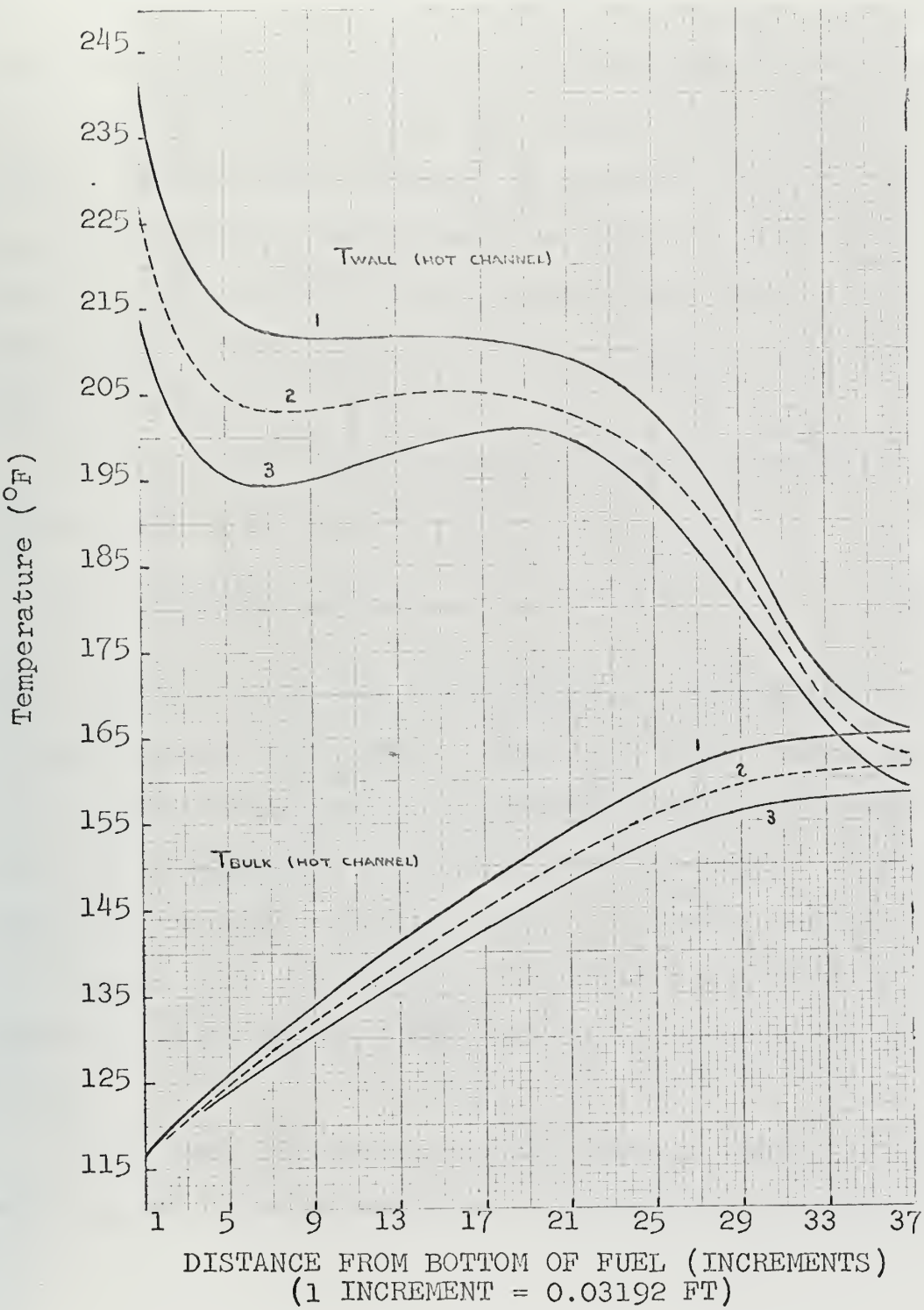

that the maximum clad wall temperature and incipient boiling temperature are equal, calculations were also made for inlet temperatures of 125°F and 135°F for the case when the shim blade height is 6.70 inches, reactor power is 6 megawatts, primary coolant flow rate is 1800 GPM, and hot channel factors are included. By plotting $(T_{wall})_{max}$ and T_{WIB} against inlet temperature, as shown in Figure 4.3, it can be concluded that the maximum allowable bulk inlet temperature, which satisfies the no-boiling requirement, is 135°F (57.2°C).

The relation between the total power, P_T, and the total coolant flow rate, W_T, is

$$P_T = C_p W_T (T_{out} - T_{in}) \quad . \qquad (4.7)$$

For a limiting flow rate of 1800 GPM, a reactor power of 6 megawatts (of which 95% is removed by the primary coolant), and an inlet temperature of 135°F, Eq. (4.7) yields the limiting reactor bulk coolant outlet temperature of 155°F (68.4°C) under the assumption that the heat capacity, C_p, is constant over the temperature ranges considered. (A value of 1.0005 BTU/lb°F was used as a conservative value of C_p.)

A low flow limitation of 1800 GPM of primary coolant would appear to be reasonable. Although the coolant pumps

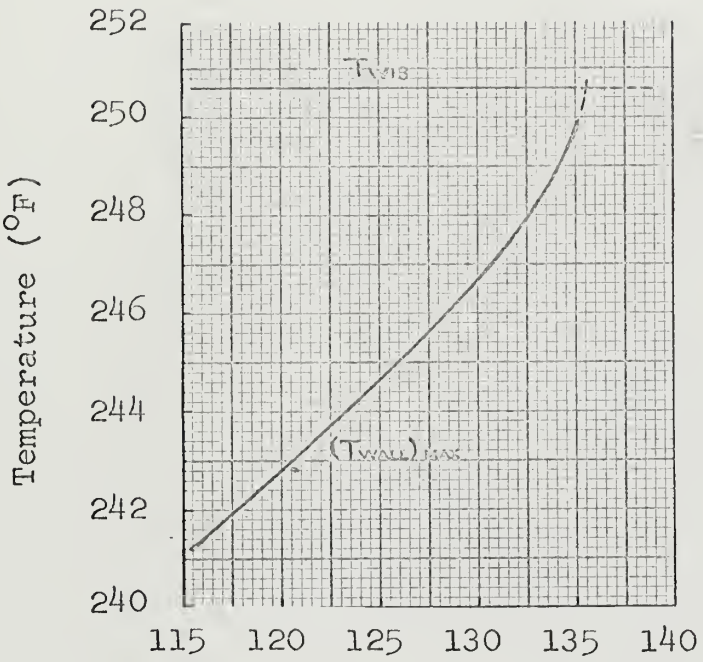

Figure 4.3

MAXIMUM CLAD WALL AND INCIPIENT BOILING TEMPERATURES

VS

BULK INLET TEMPERATURE

are able to produce a flow rate of the order of 2400 GPM, the calculations have been based on a minimum flow limit of 1800. Normal operation should easily exceed 2000 GPM, however.

Chapter 5

SECONDARY COOLANT SYSTEM

Introduction

An evaluation of the performance of the secondary coolant system at five megawatts of reactor power is described in this chapter. On the basis of this evaluation, recommendations are given as to the installation of any new components needed.

5.1 Reactor Heat Load

Two parallel heat removal systems are used to carry away the reactor heat load removed by the primary H_2O system. In this situation, each of the present heat exchangers must be so operated as to remove approximately 2.5 megawatts. To determine the required flow rate of the secondary coolant for five megawatt operation, it is necessary to investigate the efficiency of the heat exchangers at their present operating level.

The most important characteristic of the heat exchangers is its overall resistance to heat flow, 1/UA,

$$\frac{1}{UA} = \frac{1}{h_i A_i} + \frac{1}{h_o A_o} + \frac{1}{h_{sc} A_{sc}} + \frac{\ln(r_o/r_i)}{2\pi KLN} , \qquad (5.1)$$

where $1/h_i A_i$ is the convective resistance on the inside of the heat exchanger tubes, $1/h_o A_o$ is the convective resistance

on the outside of the tubes, $1/h_{sc}A_{sc}$ is the resistance of the scale on the outside of the tubes, and $\ln(r_o/r_i)/2\pi KLN$ is the conduction resistance of the walls of the tubes.

The general heat transfer relation is:

$$Q = UA\Delta T_{LM} , \tag{5.2}$$

where

$$\Delta T_{LM} = \frac{\Delta T_1 - \Delta T_2}{\ln\left[\frac{T_{11}-T_{22}}{T_{12}-T_{21}}\right]} , \tag{5.3}$$

T_{ij} = temperature of the coolant in system i at location j, i.e.,

i = 1 implies the primary system,

i = 2 implies the secondary system,

j = 1 implies the heat exchanger inlet

j = 2 implies the heat exchanger outlet, and

$\Delta T_1 = T_{11} - T_{12}$, etc.

The relations

$$Q = C_p W_i \Delta T_i \tag{5.4}$$

are used to determine the flow rate, W_i, necessary to remove the heat load Q with a temperature difference, ΔT_i, across each side of the heat exchanger.

Consistent with the limiting nature of this study, the secondary H_2O flow rate was computed for conditions which

would exist on the hottest day. The outlet temperature of the cooling towers was taken to be 92.75°F (see Chapter 6) with a reactor power of 5 Mw and outlet temperature of 155°F. Then at the normal total primary flow rate of 2000 GPM, the ΔT_1 across the core becomes 15.1°F and the reactor inlet temperature is 139.9°F. To compute the heat exchanger performance, it must be remembered that both heat loads and flow rates are taken to be half their total values as only one of the two paralled and identical systems is being considered.

In Eq. (5.1), h_i can easily be calculated by a well-correlated expression and the conduction term is well known. The principal unknowns are h_o and $h_{sc}A_{sc}$. According to McAdams (20),

$$h_i = \frac{K}{D_i}(0.023Re^{0.8}Pr^{0.33}) , \qquad (5.5)$$

and h_o can be approximated by

$$h_o = C(KRe^{0.6}Pr^{0.33}) . \qquad (5.6)$$

Devoto (21) performed heat exchanger experiments to determine the values of $h_{sc}A_{sc}$ and the product C x K in Eq. (5.6), the results of which are given in Table 5.1. The values of $(h_{sc}A_{sc})^{-1}$ and C x K determined by Devoto are essentially constant over the ranges of temperature (50 to 200°F) and flow rate (500 to 1200 GPM per heat exchanger) considered.

Table 5.1 also lists the other parameters necessary for the heat exchanger calculations.

A sample calculation is presented below based on the parameters given in Table 5.1. The value of the secondary H_2O flow rate was derived by an iterative solution to the overall heat balance based on an inlet temperature to the heat exchanger consistent with the cooling tower outlet temperature on the hottest day and an approximate value of the average secondary bulk coolant temperature.

5.1.1 Conductive Resistance

With the parameters taken from Table 5.1,

$$\frac{\ln(r_o/r_i)}{2\pi KLN} = \frac{\ln(0.0156/0.0115)}{2\pi(9.4)(14.17)(885)} = 4.117 \times 10^{-7} \frac{hr^oF}{BTU} .$$

5.1.2 Inside Convective Resistance

Using Eq. (5.5) and the values of the parameters listed in Table 5.1, the value of h_i was computed on the basis of one tube:

$$Re = \frac{W_i D_i}{A_x \mu} ,$$

$$W_i = \frac{(1000)(8.1745)(60)}{885 \text{ tubes}} = 554.2 \frac{lb}{hr \text{ tube}} ,$$

$$Re = \frac{(554.2)(0.023)}{(0.000395)(1.072)} = 3.0103 \times 10^4 ,$$

Table 5.1

PARAMETERS FOR HEAT EXCHANGER CALCULATIONS

Tube length	L	14.17 ft
Inside tube radius	r_i	0.0115 ft
Outside tube radius	r_o	0.0156 ft
Tube wall thickness	x	0.00408 ft
Pitch	P_T	0.04167 ft
Outside wall area of tubes	A_o	1230.50 ft^2
Inside wall area of tubes	A_i	909.88 ft^2
Cross section of one tube	A_x	0.000395 ft^2
Average primary bulk temperature		147.5°F
Average secondary bulk temperature (approximate)		102°F
K (stainless steel)		9.4 BTU/hr ft°F
W_1 = 1000 GPM per heat exchanger		
W_2 = 690 GPM per heat exchanger		
H_2O properties:		
Pr (102°F)		4.42
Pr (147.5°F)		2.80
μ (102°F)		1.617 lb/hr ft
μ (147.5°F)		1.072 lb/hr ft
w (102°F)		8.2723 lb/gal
w (147.5°F)		8.1745 lb/gal
$(h_{sc}A_{sc})^{-1}$		13.677 x 10^{-7} hr°F/BTU
C x K		0.33 BTU/hr ft^2°F

$Re^{0.8} = 3827.23,$

$Pr^{0.33} = 1.405,$ and

$$h_i = \frac{K}{D_i}(0.023\ Re^{0.8}Pr^{0.33}) =$$

$$\frac{(0.3836)(0.023)(3827.23)(1.405)}{(0.023)}$$

$$h_i = 2062.71 \text{ BTU/hr ft}^{2o}\text{F} .$$

With this value of h_i, the value of $(h_iA_i)^{-1}$ was calculated, and found to be:

$$(h_iA_i)^{-1} = [(2062.71)(909.88)]^{-1} = [1.877 \times 10^6]^{-1} , \text{ or}$$

$$(h_iA_i)^{-1} = 5.328 \times 10^{-7} \text{ hr}^{o}\text{F/BTU}.$$

5.1.3 Outside Convective Resistance

In order to calculate the value of h_o, the equivalent diameter of the tubes must be known to calculate the Reynolds Number. The expression for the equivalent diameter, D_e, (22) is:

$$D_e = \frac{4(P_T^2 - \pi r_o^2)}{\pi d_o} = \frac{2(P_T^2 - \pi r_o^2)}{\pi r_o} . \qquad (5.7)$$

Using the values of the parameters listed in Table 5.1, and Eqs. (5.6) and (5.7), the value of h_o was calculated as follows:

$$D_e = \frac{2(17.361 - 7.645) \times 10^{-4}}{4.901 \times 10^{-2}} = 3.965 \times 10^{-2} \text{ ft},$$

$$W_o = \frac{(690)(8.2723)(60)}{885} = 386.98 \frac{lb}{hr\ tube},$$

$$R_e = \frac{(386.98)(0.03965)}{(0.000395)(1.617)} = 2.4022 \times 10^4,$$

$$Re^{0.6} = 424.98,$$

$$Pr^{0.33} = 1.633, \text{ and}$$

$$h_o = (0.33)(1.633)(424.98) = 229.02 \text{ BTU/hr ft}^{2o}\text{F}.$$

With this value of h_o, the value of $(h_oA_o)^{-1}$ was calculated, and found to be:

$$(h_oA_o)^{-1} = [(229.02)(1230.5)]^{-1} = [2.818 \times 10^5]^{-1}$$

$$(h_oA_o)^{-1} = 35.486 \times 10^{-7} \text{ hr}^o\text{F/BTU}.$$

Combining all of the resistance terms, the value of $(UA)^{-1}$ is:

$$(UA)^{-1} = (4.117 \times 13.677 + 5.328 + 35.486) \times 10^{-7} = 58.608 \times 10^{-7} \text{ hr}^o\text{F/BTU}.$$

By combining the primary and secondary coolant heat load equations, i.e., Eq. (5.4), ΔT_2 was found to be:

$$\Delta T_2 = \frac{W_1}{W_2}\Delta T_1 = \frac{1000}{890}(15.1) = 16.97^o\text{F}$$

assuming the densities and heat capacities of the coolant in each system are equal. Using Eq. (5.3) and solving for T_{22} and ΔT_{LM} yielded:

$$T_{22} = T_{21} + \Delta T_2 = 92.75 + 16.97 = 109.72^o\text{F}$$

and

$$\Delta T_{LM} = \frac{15.1 - 16.97}{\ln\left[\frac{155 - 109.72}{139.9 - 92.75}\right]} = 46.21^o\text{F}.$$

Combining the heat load and ΔT_{LM} computed above into Eq. (5.2), the calculated value of $(UA)^{-1}$ is found to be

$$(UA)^{-1} = \Delta T_{LM}/Q = 58.81 \times 10^{-7} \text{ hr}^{\circ}\text{F/BTU}$$

which is in good agreement with the value of $(UA)^{-1}$ found by adding the individual resistance terms.

In summary, it may be concluded that a minimum, total secondary coolant flow rate of 1380 GPM is sufficient to remove the 5 Mw reactor heat load on the "hottest day".

5.2 D_2O Reflector Heat Load

In Section 4.3 it was shown that the reflectors and shield absorbed 6.63% of the energy released in the reactor. For a conservative basis in determining the operational limits of the core and primary coolant system, a fraction of the heat generated in the reflectors and shield was assumed to be conducted into the core tank where it was removed by the primary coolant system.

If none of the heat generated in the reflectors and shield is conducted into the core tank, then approximately five percent of the energy released in the reactor must be carried away by the D_2O reflector heat removal system. This is a conservative estimate since the heat dissipated in the shield is expected to be approximately 1.63% of the reactor power (see Section 5.3 below).

The D_2O reflector heat removal system is currently being designed upon the 250 kilowatt heat load requirement. Specifications for the D_2O reflector heat exchanger call for the transfer of 850,000 BTU/hr with a primary outlet temperature of 100°F, a secondary inlet temperature of 80°F, and with primary and secondary flow rates of 180 GPM in each system. These specifications are conservative, and are sufficient to remove the D_2O reflector heat load.

5.3 Shield Heat Load

The shield coolant system removes the heat deposited in the lead thermal shield which surrounds the graphite reflector and the thermal column. It is assumed that the primary contribution to heating in the thermal shield comes from the energy deposited by gamma radiation and neutron interaction in the boral, with only a very small amount of heat introduced by conduction from the graphite reflector.

Stainless steel coils embedded in the vertical cylindrical shield, the bottom shield, the lower annular ring shield, and the shield surrounding the thermal column are used for heat removal. Each individual cooling coil is equipped with a flow control valve at the inlet to allow for individual flow regulation. The total coolant flow rate through the heat removal coils is 108 GPM. The coolant passes through the shell side of the shield coolant heat exchanger where the heat is transferred to the secondary H_2O coolant system; the

secondary H_2O coolant flow rate through the tube side of the shield coolant heat exchanger is approximately 60 GPM.

The flow rates stated above are sufficient to remove the heat deposited (120 kilowatts or 2.4% of the total reactor power) in the shield with the MITR-I core, and to avoid excessive shield temperatures which would cause cracking of the concrete. The heat load expected for the MITR-II core is less than that for the MITR-I core (23), hence the existing shield coolant system is sufficient to remove the shield heat load.

Chapter 6

COOLING TOWERS

Introduction

The thermal equilibrium temperature of the entire reactor is dependent on the temperature of the H_2O secondary coolant leaving the cooling towers. An evaluation of the performance of this equipment is therefore vital to this study of process system requirements.

6.1 Complicating Factors

Any analysis of the cooling towers is complicated by the following factors:

1) The total flow through the cooling towers is inaccurately known. The H_2O secondary coolant removes heat from the following items:
   a) the H_2O primary coolant heat exchangers 1 and 1A,
   b) the H_2O primary coolant cleanup heat exchanger 2,
   c) the shield coolant heat exchanger 3,
   d) the experimental coolant heat exchanger 4,
   e) the D_2O reflector heat exchanger D-1,
   f) the D_2O reflector cleanup heat exchanger D-2, and
   g) three air conditioning units which vary in size from three to twenty tons.

There are four flow meters which monitor the flow through each of the systems listed above with the exception of the air conditioning units, however, only one flow meter is used to monitor the common flow through heat exchangers 2, 3, 4, D-1 and D-2. One flow meter, connected to the 10 inch influent line leading to the cooling towers is not used. The remaining two flow meters monitor the flow through each of the H_2O primary coolant heat exchangers. The only method of estimating the total H_2O flow is to close off all systems except the main heat exchangers and then measure the flow through these units. This method is not exact since the pressure drops throughout the various systems are not matched to the pressure drop across heat exchangers 1 and 1A.

2) Heat exchanger no. 1 will be replaced by a newer heat exchanger of larger capacity.

3) The temperature of the water entering the cooling towers is not accurately known. Since the secondary coolant system has so many branches and functions, the various outlet temperatures should be combined in a volume average to calculate the temperature of the water entering the

towers. This is not possible, however, as much of this information is not available.

4) The cooling tower performance is dependent on such quantities as ambient temperature, relative humidity, and wind velocity which are constantly changing.

6.2 Secondary Coolant Requirements

Design specifications for each of the cooling towers call for 1000 GPM of H_2O to be cooled from 103°F to 80°F at a maximum wet-bulb temperature of 72°F and 0 to 10 MPH wind. The flow rate going to the top of the cooling towers is approximately 1600 GPM (800 GPM per tower).

Devoto (24) developed an empirical equation, given below, which was based upon the conclusion that the water temperature leaving the cooling tower is dependent only on the wet bulb temperature and reactor power level.

$$T_{H1} = T_{WET} + CP_T \qquad (6.1)$$

where: T_{H1} = cooling tower outlet temperature, °F

T_{WET} = wet-bulb temperature, °F

C = constant = 4.5°F/Mw (per tower)

P_T = reactor power, Mw.

Equation (6.1) was derived for one cooling tower and the primary coolant heat exchanger 1. No specific data has been taken since the addition of the second cooling tower

and heat exchanger 1A, but after reviewing current reactor operating logs and U.S. Weather Bureau (Boston) meteorological data and changing the constant to account for two cooling towers, Devoto's empirical relation still shows a good correlation of the parameter involved, i.e.,

$$T_{H1} = T_{WET} + C'P_T \qquad (6.2)$$

where: $C' = 2.25^{\circ}F/Mw$ (for both towers).
When heat exchanger 1 is replaced with the newer heat exchanger of larger capacity. Eq. (6.2) should be rechecked.

On a hypothetical "hottest day", a wet-bulb temperature of $78^{\circ}F$ corresponding to an air temperature of $78^{\circ}F$ at 100 percent relative humidity, the cooling towers outlet temperature would be approximately $95^{\circ}F$ (allowing for an additional $3.5^{\circ}F$ temperature increase due to the air conditioning units) with a reactor power level of 6 Mw. Since this is less than the limiting reactor inlet temperature derived in Section 4.5, the secondary system is believed to be adequate for 5 Mw operation of the MITR-II.

Chapter 7

SUMMARY AND RECOMMENDATIONS

7.1 Summary

To determine the process system operating limits of the MITR-II, the nuclear properties of the reactor were examined first in order to study the power production within the core as a whole and within a single fuel element. The results of computer code calculations were used to investigate the effects of control rod height on the relative variations in the radial and axial neutron flux and power density distributions. Emphasis of the study centered on the hottest element and, further, the hottest fuel plate.

An independent series of experiments produced a well-correlated value for the coefficient of convective heat transfer on the surface of the finned fuel element plates. The derivation of this heat transfer coefficient has been studied and incorporated into the fuel plate temperature calculations.

Engineering hot channel factors have been established to account for small dimensional deviations from the nominal design of the reactor fuel elements resulting from manufacturing tolerances, for departures from ideal flow conditions, and for uncertainties in power, flow, and heat transfer measurements.

When the power density distributions, coefficient of convective heat transfer, and engineering hot channel factors were coupled together with the thermal hydraulic properties of the coolant and fuel element and the coolant flow rate, the location of the hottest fuel plate surface temperature was determined. The temperature at this location was limited by the requirement that no boiling of any type occur in the core. A limitation was then placed on the maximum bulk coolant temperature under the most adverse operating conditions. Once reasonable ranges of values of these parameters were established, then, limits on the measurable parameters, i.e., minimum coolant flow rate, maximum bulk outlet temperature, and maximum reactor power, were established such that the reactor could be operated with these parameters simultaneously approaching their limits.

Attention was next given to the secondary coolant system that is used to remove the heat generated in the core, D_2O reflector, and shield, by using cooling towers, in order to have the reactor facility operate efficiently. Two parallel heat removal systems are used to carry away the heat load removed by the primary H_2O system. To determine the required flow rate of the secondary coolant for five megawatt operation, it was necessary to investigate the efficiency of the main heat exchangers at their present operating level while remaining consistent with the limiting nature of this study. The flow

rate on the secondary side of the heat exchangers necessary to maintain the correct reactor operating conditions under the most severe limitations on heat removal was calculated after performing several iterations to determine the variation of the overall coefficient of heat transfer with flow rate and a known amount of heat.

Although most of the heat generated in the MITR-II is removed by the primary coolant, a small percentage of the heat load is carried away by the heavy water (D_2O) in the inner reflector and by the distilled H_2O in the shield coolant system. These systems have their own separate heat exchangers. The amount of heat carried away by each of these systems was also examined. On the basis of these examinations, recommendations are made as to the equipment necessary to remove each of the heat loads.

The thermal equilibrium temperature of the entire reactor is dependent on the temperature of the secondary H_2O coolant leaving the cooling towers. An evaluation of the performance of this equipment was therefore vital to this study. The most adverse conditions of temperature, relative humidity, and reactor power level were used for this study, and the maximum temperature of the water supplied to the secondary cooling system at five megawatts was determined.

Section 7.2 of this chapter is a summary of the principal results and theoretical predictions. On this basis,

conclusions are drawn, and recommendations are made and outlined in Section 7.3. It must be emphasized at the outset that this is essentially a limiting study to determine the limiting safety system settings of the MITR-II. In all assumptions and calculations, the safest or most conservative choice has been selected. The most severe hazards of weather and operating conditions have been envisioned and employed throughout.

7.2 Results

The principal results of this study are:

1) From the standpoint of process system operating limits, a maximum reactor power level setting of six megawatts (total) was established so that automatic protective action would correct the most severe abnormal power level deviation anticipated before a safety limit is exceeded.

2) The minimum allowable H_2O primary coolant flow rate for six megawatts was set at 1800 GPM. It was anticipated that the normal flow rate should easily exceed 2000 GPM.

3) The maximum allowable temperature of the fuel plate clad at the hottest point (lower end of the fuel plate) in the core was found to be 250.6°F, and the value of the maximum bulk coolant temperature at the reactor outlet was established at 155°F.

4) It was established that the flow rate in the secondary H_2O coolant system necessary to remove the 5 Mw reactor heat load was approximately 1380 GPM on the postulated "hottest day".

5) A heat exchanger capable of transferring 850,000 BTU/hr with a primary D_2O flow rate of 180 GPM and outlet temperature of $100^{\circ}F$ and with a secondary H_2O flow rate of 180 GPM and inlet temperature of $80^{\circ}F$ would be sufficient to remove the D_2O reflector heat load.

6) It was established that the existing shield coolant system would maintain satisfactory shield temperatures so as to prevent cracking of the concrete and remove the heat load in the shield.

7) The cooling towers were shown to be adequate to deliver H_2O to the secondary coolant system at a maximum temperature of $92.75^{\circ}F$ with the reactor power level of 5 Mw on a postulated "hottest day".

7.3 Recommendations

On the basis of the investigations made for this study, it is recommended that:

1) The process system operating limits as determined herein be incorporated as the Limiting Safety System Settings of the MITR-II.

2) Upon the replacement of the H_2O primary coolant Heat Exchanger No. 1 and the shield coolant Heat Exchanger No. 3 and upon the addition of the D_2O reflector Heat Exchanger No. D-1, experiments be conducted to accurately determine the overall resistance to heat flow, $(UA)^{-1}$.

Appendix A

NOMENCLATURE

a	fuel clad thickness
A	area, general
A_i	inside wall area of heat exchanger tubes
A_o	outside wall area of heat exchanger tubes
A_p	clad back plate area
A_x	cross-sectional area of one heat exchanger tube
b	fuel plate meat half-thickness
C	constant, $4.5^{o}F/Mw$
C'	constant, $2.25^{o}F/Mw$
CxK	constant, 0.33 BTU/hr $ft^{2o}F$
C_p	specific heat
d	channel thickness
d_o	O.D. of heat exchanger tube
D_e	equivalent flow diameter
E	total energy released per fission
E_c	energy released per fission resulting from neutrons being captured in materials of the reactor
F_a	axial power factor
F_H	enthalpy hot channel factor
F_Q	heat flux hot channel factor
F_r	radial power factor
F_Θ	film temperature difference hot channel factor

h	convective heat transfer coefficient
K	constant, $3.3095 \times 10^{-17} \frac{\text{Mw-sec}}{\text{fission}}$ (Chapter 3)
K	thermal conductivity, general
K_c	thermal conductivity of clad
K_M	thermal conductivity of fuel meat
L	length of tube in heat exchanger
N	total number of tubes in heat exchanger
Nu	Nussult number
P	power
P	pressure
P	wetted perimeter
P_T	pitch
P_T	total power
PAV	average power density
PDM	power density in fuel meat
Pr	Prandtl number
q	heat load, BTU/hr
q''_{AVG}	average heat flux, BTU/hr ft^2
q''_{IB}	heat flux at incipient boiling
Q	heat load or power
Q/A	heat flux
r_i	inside radius of heat exchanger tube
r_o	radius
Re	Reynolds number
t_{eff}	thickness of equivalent flat plate test section
T	temperature
T_{H1}	cooling tower outlet temperature

ΔT temperature difference

ΔT_{LM} log-mean temperature difference

T_{SAT} fluid saturation temperature

T_{wall} clad surface temperature

T_{WIB} clad surface temperature (local) at incipient boiling

U overall coefficient of heat transfer

v fluid velocity

V volume, general

V_i volume fraction of material i (Chapter 4)

V_i volume of i^{th} fuel region (Chapter 3)

w density, lb/gal

W flow rate

W_T total flow rate

x thickness of tube in heat exchanger

α alpha particle

β beta particle

β reactivity value relative to the delayed neutron fraction. The value of β is estimated to be approximately 0.0075 K_{eff} for this reactor, including the delayed photoneutrons.

γ gamma radiation

η fin effectiveness defined as the ratio the effective area of the finned plate surface to the area of the back plate surface viscosity

μ	viscosity
μ	effective linear absorption coefficient
μ_i	linear absorption coefficient of material i
ρ	density
Σ	summation
$\Sigma_{absorption}$	macroscopic absorption cross section
$\Sigma_{capture}$	macroscopic capture cross section
Σ_f	macroscopic fission cross section
$\Sigma_{f_{ij}}$	macroscopic fission cross section in i^{th} fuel region and j^{th} energy group
Σ_{rl}	macroscopic removal cross section for fast neutrons
ϕ	neutron flux
ϕ_l	fast neutron flux
$\bar{\phi}_{ij}$	volume averaged neutron flux in the i^{th} fuel region and j^{th} energy group

FOOTNOTES

1. Addae, A.K., "The Reactor Physics of the MIT Reactor Redesign", MIT Department of Nuclear Engineering, ScD Thesis, June 1970.

2. Fowler, T.B., Tobias, M.L., and Vondy, D.R., "Exterminator-2: A Multigroup Code for Solving Neutron Diffusion Equations in One and Two Dimensions", ORNL-TM-842, July 1966.

3. Etherington, H., ed., Nuclear Engineering Handbook, McGraw-Hill Book Co., New York, 1958, p. 2-2.

4. Rockwell, T., ed., Reactor Shielding Design Manual, D. VanNostrand Company, Inc., Princeton, New Jersey, 1956, p. 34.

5. Glasstone, S. and Sesonske, A., Nuclear Reactor Engineering, D. VanNostrand Company, Inc., Princeton, New Jersey, 1963, pp. 16-98.

6. Bonilla, C.F., Nuclear Engineering, McGraw-Hill Book Co., New York, 1957, p. 5.

7. Rasmussen, N.C., Private Communication (MIT Nuclear Engineering Department Report to be published).

8. Glasstone, S. and Sesonske, A., op cit., p. 341.

9. Rasmussen, N.C., op cit.

10. Ibid.

11. Ibid.

12. Etherington, H., op cit., p. 7-74.

13. Addae, A.K., op cit.

14. Cadwell, W.R., "PDQ-7 Reference Manual", WAPD-TM-678, January 1967.

15. Spurgeon, D.R., "Preliminary Design Studies for a High Flux MIT Reactor", MIT Nuclear Engineering Department, SM and Nuclear Engineers Thesis, May 1969.

16. Furtado, P.M., "Longitudinally Finned Test Section Experimental Data Analysis", MIT Nuclear Engineering Department (Unpublished).

17. Miller, R.W., et al, "Report of the SPERT I Destructive Test Program on an Aluminum, Plate-type, Water-moderated Reactor", IDO-16883, 1964.

18. Reactor Shielding, International Atomic Energy Agency, Technical Series No. 34, Vienna, 1964, pp. 228-229.

19. Griebenow, M.L. and Richert, K.D., "Macabre II", Idaho Nuclear Corporation, TID-4500, September 1967.

20. McAdams, W.H., Heat Transmission, McGraw-Hill Book Co., New York, 1954, p. 425.

21. Devoto, W.R., "Process System Requirements of the MIT Reactor at Five Megawatts", MIT Nuclear Engineering Department, SM and Nuclear Engineers Thesis, MITNE-23, August 1962, p. 109.

22. Kern, D.Q., Process Heat Transfer, McGraw-Hill Book Co., New York, 1950, p. 138.

23. Choi, D.K., "Temperature Distribution and Natural Convective Shutdown Cooling of the MITR-II", MIT Nuclear Engineering Department, SM Thesis, May 1970.

24. Devoto, W.R., op cit., p. 153.

BIBLIOGRAPHY

Addae, A.K. and Thompson, T.J., "Reactor Physics Considerations of the MIT Reactor Redesign", MIT Nuclear Engineering Department, (a paper presented at the American Nuclear Society 1969 Winter Meeting, San Francisco).

Bonilla, C.F., Nuclear Engineering (McGraw-Hill Book Company, Inc., New York, 1957).

Devoto, W.R., "Process System Requirements of the MIT Reactor at Five Megawatts", MIT Nuclear Engineering Department, (S.M. and Nuclear Engineers Thesis, MITNE-23, Cambridge, Mass., 1962).

Etherington, H., ed., Nuclear Engineering Handbook, (McGraw-Hill Book Company, Inc., New York, 1958).

Kern, D.Q., Process Heat Transfer, (McGraw-Hill Book Company, Inc., New York, 1950).

LeTourneau, B.W. and Grimble, B.W., "Engineering Hot Channel Factors for Nuclear Reactor Design", (Nuclear Science and Engineering: 1, 359-369, 1956).

McAdams, W.H., Heat Transmission, (McGraw-Hill Book Company, Inc., New York, 1954).

Rockwell, T., ed., Reactor Shielding Design Manual, (D. VanNostrand Company, Inc., New Jersey, 1956).

Rohsenow, W.M. and Choi, H., Heat, Mass, and Momentum Transfer, (Prentice-Hall, Inc., New Jersey, 1961).

Wolak, F.A., "Heat Dissipation in the MIT Reactor", MIT Nuclear Engineering Department, (SM Thesis, Cambridge, Mass. 1958).

Thesis 118386
L95 Luxford
Process system safety
limits of the MITR-II.